Quaternary Science Reviews 216 (2019) 74–88

Contents lists available at ScienceDirect

Quaternary Science Reviews

journal homepage: www.elsevier.com/locate/quascirev

History of Yellow River and Yangtze River delivering sediment to the Yellow Sea since 3.5 Ma: Tectonic or climate forcing?

Jin Zhang [a, c], Shiming Wan [a, b, d, *], Peter D. Clift [e], Jie Huang [a], Zhaojie Yu [a], Kaidi Zhang [a], Xi Mei [f], Jian Liu [f], Zhiyong Han [g], Qingyun Nan [a], Debo Zhao [a], Anchun Li [a], Lihui Chen [h], Hongbo Zheng [i], Shouye Yang [j], Tiegang Li [k], Xunhua Zhang [l]

[a] Key Laboratory of Marine Geology and Environment, Institute of Oceanology, Chinese Academy of Sciences, Qingdao 266071, China
[b] Laboratory for Marine Geology, Qingdao National Laboratory for Marine Science and Technology, Qingdao 266061, China
[c] University of Chinese Academy of Sciences, Beijing 100049, China
[d] CAS Center for Excellence in Quaternary Science and Global Change, Xi'an 710061, China
[e] Department of Geology and Geophysics, Louisiana State University, Baton Rouge, LA 70803, USA
[f] Key Laboratory of Marine Hydrocarbon Resources and Environmental Geology, Ministry of Land and Resources, Qingdao Institute of Marine Geology, Qingdao 266071, China
[g] School of Geographic and Oceanographic Sciences, Nanjing University, Nanjing 210023, China
[h] State Key Laboratory for Mineral Deposits Research, School of Earth Sciences and Engineering, Nanjing University, Nanjing 210023, China
[i] Research Center for Earth System Science, Yunnan University, Kunming 650500, China
[j] State Key Laboratory of Marine Geology, Tongji University, Shanghai 200092, China
[k] Key Laboratory of Marine Sedimentology and Environmental Geology, First Institute of Oceanography, State Oceanic Administration, Qingdao 266061, China
[l] Nanjing Center, China Geological Survey, Nanjing 210016, China

ARTICLE INFO

Article history:
Received 11 February 2019
Received in revised form
30 May 2019
Accepted 2 June 2019
Available online 13 June 2019

Keywords:
Clay minerals
Sr-Nd isotopes
Provenance
Yellow River (Huanghe) and Yangtze River (Changjiang)
Yellow Sea
Quaternary

ABSTRACT

Reconstructing the Plio-Pleistocene sedimentary history of the Yellow Sea, is important for understanding the long-term influence of the Yellow River (Huanghe) and/or Yangtze River (Changjiang) on the Asian marginal seas and to further constrain any links between river development, regional paleoenvironmental change, tectonic deformation and/or global climate change. Here we present the first high-resolution clay mineral record combined with Sr-Nd isotopic compositions from a 300-m long sediment core recovered in the western South Yellow Sea. Our study suggests that large-scale transgression in the Yellow Sea occurred after ~0.8 Ma, possibly related to tectonic subsidence of eastern China coast and the Min-Zhe Uplift. In contrast, the sedimentary environment of Bohai and Yellow Seas was mainly dominated by fluvial/lacustrine deposits at 3.5–0.8 Ma. Provenance analysis suggests a major change in sediment provenance from the Yangtze River to the Yellow River at ~0.8 Ma, which corresponds to the timing of the final integration of the Yellow River in its present form. At the same time the major channels of the Yangtze River migrated from the South Yellow Sea to the modern Yangtze River delta due to the subsidence of east China coast. The consistence in timing of the provenance transition and large-scale regional marine transgression suggests that tectonic deformation, rather than climate change, is the first-order control on the evolution of the Yellow and Yangtze Rivers and sedimentary environmental change in the Bohai and Yellow Seas.

1. Introduction

The stepwise uplift of the Himalaya and Tibetan Plateau (HTP), following the start of India-Eurasia continental collision at 50–60 Ma, has been suggested to have significantly influenced the long-term evolution of Asian topography, rivers, the monsoon system and even global climate (Clift et al., 2008; Wang, 2004). The East Asian marginal seas are not only closely linked to India-Eurasia collision and Pacific subduction (Ren et al., 2002), but are also major sinks of sediment eroded from river drainage basins onshore

* Corresponding author. Key Laboratory of Marine Geology and Environment, Institute of Oceanology, Chinese Academy of Sciences, Qingdao 266071, China.
E-mail address: wanshiming@ms.qdio.ac.cn (S. Wan).

https://doi.org/10.1016/j.quascirev.2019.06.002
0277-3791/

(Milliman and Farnsworth, 2011). As a result this is a critical area for studying the evolution of large Asian river systems and their sedimentary response, as well as for understanding land-sea and tectonic-climate interactions (Deng et al., 2017; Zheng et al., 2013). However, it remains controversial how, when and why the Yellow and Yangtze Rivers began to influence the East Asian marginal seas, largely because of the lack of long and well-dated sedimentary archives that span tectonic time scales (Yao et al., 2017).

The Yellow and Yangtze Rivers originate from the Tibetan Plateau (Fig. 1), flow into the East Asian marginal seas and account for approximately 8% of the modern global terrigenous material to the ocean (Milliman and Farnsworth, 2011). Previous studies showed that the timing of final integration of the Yellow River ranges from the Eocene (Lin et al., 2001), to the late early Pleistocene (e.g., Hu et al., 2017; Yang et al., 2001; Yao et al., 2017) or even the late Pleistocene (e.g., Jiang et al., 2007). In contrast, it has been argued that the Yangtze River was integrated close to its present form during the Eocene (Richardson et al., 2008), the early Miocene (Clark et al., 2004; Clift et al., 2006; Zheng et al., 2013), or the late Pliocene to Pleistocene (e.g., Fan et al., 2005; Jia et al., 2010; Yang et al., 2006a). Consequently, the drainage history of the Yellow and Yangtze Rivers, especially the onset of their integration and influence over the East Asian marginal seas need to be constrained.

As one of the East Asian marginal seas the Yellow Sea is highly sensitive to sea-level fluctuations, climate change and tectonic activity, due to its wide extent and low-gradient continental shelf (e.g., Liu et al., 2016a; Liu et al., 2018; Qin et al., 1989). The Yellow Sea has been dominated by continental environments since the early Paleogene, with large scale marine transgression in the Yellow Sea only starting in the Pleistocene (Qin et al., 1989; Wang, 2004; Yi et al., 2003). However, the precise timing and origin of large scale transgression over long time scales, particularly since the Pliocene, are still unknown. Although there are lots of paleoenvironmental studies using long sediment cores in the modern Yangtze delta (Fig. 1) (e.g., Chen et al., 2014; Fan et al., 2005; Gu et al., 2014; Jia et al., 2010; Yang et al., 2006a; Yue et al., 2018), modern Yellow River delta (Liu et al., 2016b; Yang et al., 2001; Yi et al., 2016) and the Subei Plain (Wang et al., 2006), delta regions and onshore plain

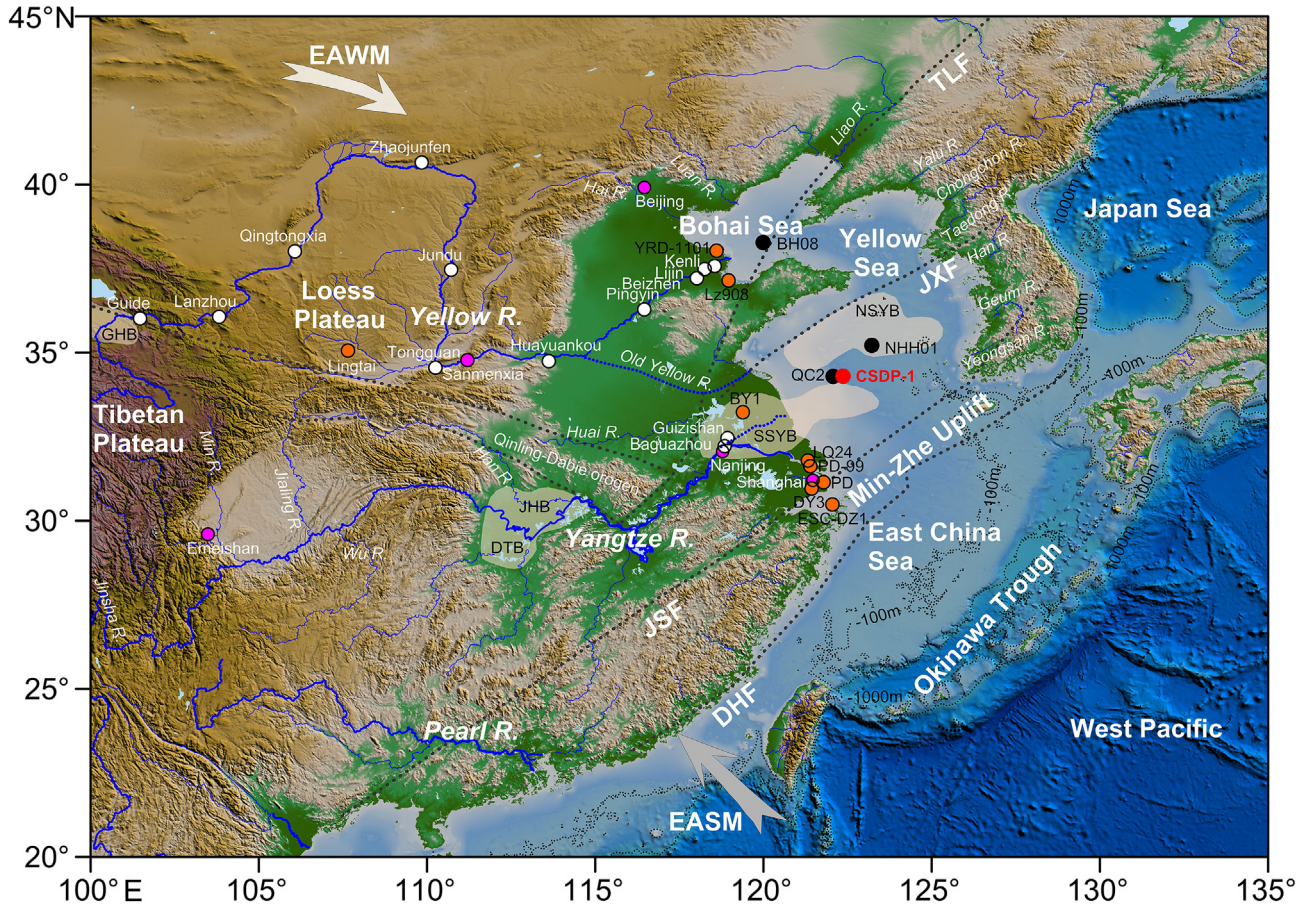

Fig. 1. Geomorphologic map of East Asia, showing the outline of major sedimentary basins, large rivers, faults, and sampled sites. Location map of Core CSDP-1 (with a red circle) in the Yellow Sea. Also the major river systems in the East Asia are shown by blue solid lines. The old Yellow River channel in AD 1128–1855 and the major paleo-Yangtze River channel in the early-middle Pleistocene are adapted from Xue (1993) and Li et al. (2011a), respectively. The East Asian Winter Monsoon (EAWM) and East Asian Summer Monsoon (EASM) are showed by white and gray arrows, respectively. −100 m and −1000 m isobaths are shown by dotted line. The −100 m isobath approximately represents the position of the shoreline during glacial lowstands. Location of offshore cores BH08 (Yao et al., 2017), NHH01 (Liu et al., 2014), QC2 (Zhou and Ge, 1990) are showed by black circle, cores onshore LQ24 (Yue et al., 2018), PD-99 (Fan et al., 2005; Yang et al., 2007b), PD (Chen et al., 2014; Gu et al., 2014), DY3 (Jia et al., 2010), ESC-DZ1 (Yi et al., 2014), BY1 (Wang et al., 2006), lz908 (Yi et al., 2016) and YRD-1101 (Liu et al., 2016b) as well as Lingtai red clay-loess profile (Sun and An, 2005) are showed by orange circle. Location of the Yellow and Yangtze Rivers sediment samples and paleo-Yangtze River sediment sample (Guizishan profile) are showed by white circle. The major sedimentary basins from north to south are the Northern South Yellow Sea Basin (NSYB) and Subei-Southern South Yellow Sea Basin (SSYB), Gonghe Basin (GHB) in the upper reach of the Yellow River, Jianghan Basin (JHB) and Dongting Basin (DTB) in the middle Yangtze River, which are shown by gray brown shadow areas. Basin locations are adapted from Wang et al. (2014) and Guo et al. (1997). The major faults systems are the Tanlu Fault (TLF), Jiaxiang Fault (JXF), Jiangshao Fault (JSF), Min-Zhe Uplift and Dongying-Haijiao Fault (DHF) (Guo et al., 1997; Wang et al., 2014). The base map data were from https://maps.ngdc.noaa.gov/viewers/wcs-client/. (For interpretation of the references to colour in this figure legend, the reader is referred to the Web version of this article.)

areas are not ideal locations to study the long-term evolution of river system and large-scale transgression of Yellow Sea because of limited accommodation space for sediments and unstable sedimentary environment (i.e., sediment reworking and changes in river channel and local geomorphology) (Chen et al., 2014; Stanley and Hait, 2000; Yue et al., 2018). More ideal area should be offshore basins in the Bohai Sea, Yellow Sea or East China Sea. Until now, there are only very few long sediment cores (>1 Ma) in these area, such as Core BH08 in the Bohai (Yao et al., 2017) and Cores QC2 (Zhou and Ge, 1990) and NH001 (Liu et al., 2014) in the Yellow Seas. Thus, the well-preserved thick sediment archive of the Yellow Sea offers a unique opportunity to study the long-term evolution of large river systems and the regional paleoenvironment, as well as their links to tectonics and/or climate change (Liu et al., 2016a, 2018).

Since 2013, Continental Shelf Drilling Program (CSDP) of China was initiated to recover a series of long sediment cores on the Chinese continental shelves by seafloor drilling in order to obtain long and continuous records of paleoenvironmental evolution of East Asian marginal seas since the Cenozoic (Liu et al., 2016a). In this study, we analyzed the clay mineralogy and Sr-Nd isotopic compositions of < 63 μm silicate sediment at drilling site CSDP-1 from the western South Yellow Sea that dates back to ~3.5 Ma. So far, this sediment core is the longest, well-dated sedimentary archive in the Yellow Sea (Liu et al., 2016a). Our objectives were to (1) reveal the sediment provenance of the core and its implications for evolution of the Yellow River and/or Yangtze River since 3.5 Ma; (2) to reconstruct the paleoenvironment change in the Yellow Sea; and (3) to understand the links between river development, regional paleoenvironmental change, tectonic activity and global climate change.

2. Geological settings of the study area

The South Yellow Sea is a semi-enclosed basin bounded by China and the Korean Peninsula. Tectonically, the South Yellow Sea is located in the eastern of lower Yangtze Block, bounded by the Jiaxiang and Jiangshao Faults on the north and south, respectively (Guo et al., 1997; Wang et al., 2014; Zhang et al., 2013) (Fig. 1). The South Yellow Sea basin is a large basin composed of a Paleozoic-Mesozoic marine sedimentary basin and a Mesozoic-Cenozoic terrigenous sedimentary basin (Zhang et al., 2013). As in other Cenozoic rift basins in East Asia, tectonic inversion and denudation also occurred in the South Yellow Sea basin from the late Eocene and/or Oligocene to the early Miocene (Yoon et al., 2010), driven by the tectonics of India-Eurasia collision and/or Pacific subduction (Ren et al., 2002).

Geophysical investigation shows that the Min-Zhe (Fujian-Zhejiang) Uplift (or Fujian-Lingnan Uplift, Zhejiang-Fujian Uplift) underlies the Yellow and East China Seas and extends from southern China to the southern Korean Peninsula (Wageman et al., 1970) (Fig. 1). The Min-Zhe Uplift mainly consists of Mesozoic to Precambrian igneous and metamorphic rocks, and is tectonically constrained by the Jiangshao Fault in the north and the Dongying-Haijiao Fault in the south (Jin, 1992; Qin et al., 1989; Wageman et al., 1970). Qin et al. (1989) and Jin (1992) inferred that the Min-Zhe Uplift was uplifted in the late Mesozoic and became a high terrain between the eastern Chinese marginal basins and the Pacific Ocean as a result of massive volcanic eruptions, and subsequently subsided from the late Pliocene to the early Quaternary. In general, the Min-Zhe Uplift appears to have a significant influence on regional geomorphology and thus act as a nature barrier against seawater intrusion from the East China Sea to the Yellow and Bohai Seas (Liu et al., 2016a, 2018; Qin et al., 1989; Zhao et al., 2019).

3. Materials and methods

Core CSDP-1 (34°18′N, 122°22′E; at ~52.5 m water depth; length 300 m; average recovery rate 80%) was retrieved from the western South Yellow Sea offshore the old Yellow River delta by Research Vessel KAN407 in June 2013 (Fig. 1). The core penetrated the entire Quaternary sequence, reaching the underlying upper Pliocene strata (~3.5 Ma) (Liu et al., 2016a). The site is located in the Yangtze Block, topographically belonging to the middle uplift zone and near to the northern edge of the southern South Yellow Sea Basin (SSYB), an offshore extension of the onshore Subei Basin (Zhang et al., 2013) (Fig. 1). The lithology of the recovered core is dominated by coastal facies, fine-grained silty terrigenous materials and fluvial facies, coarse-grained, fine-medium sandy terrigenous materials with minor calcareous biogenic components (Liu et al., 2018) (Fig. 2A–H). The chronostratigraphic framework of Core CSDP-1 was constrained by integrated magnetostratigraphy and six accelerator mass spectrometry ^{14}C dates (Liu et al., 2016a, 2018) and then linearly interpolated between these control points. The average linear sedimentation rate (LSR) is about 9.5 cm/ky. For this study, a total of 277 samples were taken at regular intervals of ~5 cm for the upper 6.7 m and ~1.8 m for the lower part of the whole core, with an average resolution of about 0.4 ky and 21.6 ky, respectively. All samples were analyzed for clay minerals and 18 samples were selected at an interval of ~17 m for the analysis of the Sr-Nd isotopic compositions of the < 63 μm silicate fraction. Dry bulk density (DBD) (g/cm^3) was measured in the laboratory of the Institute of Oceanology, Chinese Academy of Sciences (IOCAS), and the total mass accumulation rate (MAR) ($g/cm^2/ky$) was calculated by multiplying DBD by LSR based on the method of Rea and Janecek (1981).

In order to constrain the sediment provenance, an additional twenty-four samples were chosen from potential source areas. Two samples were taken from the lower reaches of the Yangtze River and sixteen from the mainstream of the Yellow River, while five loess samples were collected from the late Pliocene-Pleistocene Lingtai section of the Loess Plateau (Fig. 1). We also collected one paleo-Yangtze River sample from Guizishan profile in the major paleo-Yangtze River channel near Nanjing, which were formed during the Pliocene-middle Pleistocene (Han et al., 2009) (Fig. 1 and S1). These samples were selected to define the clay mineralogy or Sr-Nd isotopic composition of the potential source areas.

After removing organic matter and biogenic carbonate with hydrogen peroxide (15%) and acetic acid (25%), grain-size distribution measurements of the extracted terrigenous materials from Core CSDP-1 were analyzed by a CILAS 940L laser particle size analyzer at IOCAS. This apparatus accounts for grains in the range of 0.3–2000 μm and has an error below 2%. Grain-size parameters were calculated based on the methods of Mcmanus (1988), and sediment types were described and named by the Wentworth (1922) and Folk classifications (Folk et al., 1970), respectively.

Clay minerals studies were performed on the <2 μm fraction, which was separated using the Stoke's settling velocity principle, after the removal of organic matter and carbonate by 15% hydrogen peroxide and 25% acetic acid, respectively (Moore and Reynolds, 1989; Zhao et al., 2017). Clay minerals assemblages were determined by X-ray diffraction (XRD) using a D8 ADVANCE diffractometer with CuKα radiation (40 kV, 40 mA) at IOCAS. All samples were pretreated by ethylene-glycol vapor (at 60 °C, 12 h) and then measured twice: (1) over the range 3–30° 2θ at 0.02° steps; and (2) at high resolution between 24 and 26° 2θ (0.01° steps) in order to identify the 3.54/3.58 Å kaolinite/chlorite double peak (e.g., Shen et al., 2017; Zhao et al., 2017). Moreover, to verify the presence of smectite, illite, kaolinite and chlorite, four samples were air-dried

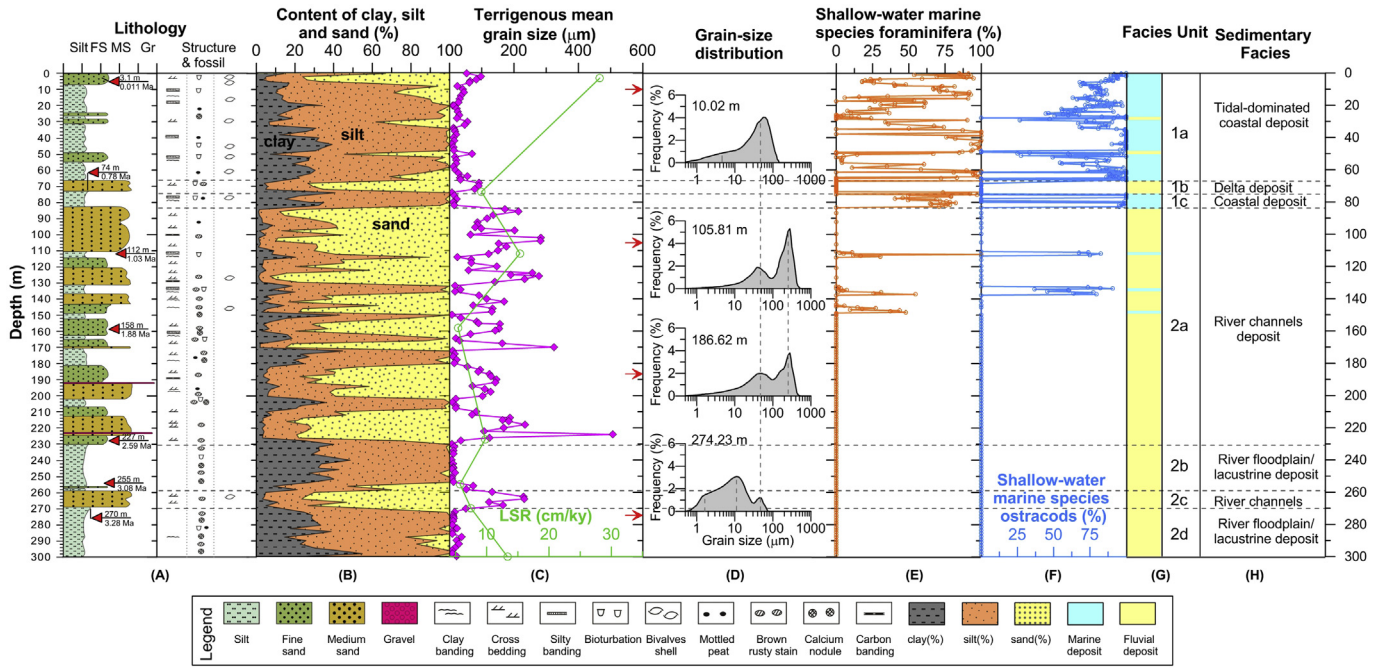

Fig. 2. Downcore changes of lithology (A), content of clay, silt and sand (B), terrigenous mean grain size and linear sediment rate (LSR) (Liu et al., 2016a) (C), grain-size distribution (D), the abundance of shallow-water marine species foraminifera relative to shallow-water euryhaline species (Liu et al., 2018) (E), the abundance of shallow-water marine species ostracods relative to shallow-water euryhaline species (Liu et al., 2018) (F), facies unit (G) and sedimentary facies (H). The characteristic of the downcore lithology was simplified from Liu et al. (2018). Ages model for Core CSDP-1 are labeled based on the chronostratigraphic framework (Liu et al., 2016a).

and heated at 490 °C for 2 h, and the clay minerals were identified based on the position of the (001) series of basal reflections on the three XRD spectra (Moore and Reynolds, 1989). Semi-quantitative estimates of the relative percentages of clay mineral assemblages were calculated from the peak areas over the basal reflection. We estimated the main clay mineral groups of smectite (including mixed-layers) (15–17 Å), illite (10 Å), and kaolinite/chlorite (7 Å) from ethylene-glycol curves by Topas 2P software using the method of Biscaye (1965). The replicate measurement error is below 5% (e.g., Shen et al., 2017). Additionally, illite chemical index was determined using the ratio of the 5 Å and 10 Å illite peak areas. Ratios of illite chemical index lower than 0.5 represent Fe-Mg-rich illite produced by weak chemical weathering conditions; ratios higher than 0.5 indicate Al-rich illite formed by strong hydrolysis (Esquevin, 1969). Illite crystallinity was calculated from the ethylene-glycol curves from the full width at half maximum height (FWHM) of the illite peak (10 Å) (Moore and Reynolds, 1989). Likewise smectite crystallinity was determined from the smectite peak (17 Å). Results are shown in Table 1. In addition, all the clay mineralogical results cited in this study have been recalculated using the approach of Biscaye (1965) so that the results can be directly compared.

Eighteen smear slides of bulk samples were observed to assess the influence of diagenetic alteration using a Zeiss polarizing microscope at IOCAS. In addition, similar micro-morphological studies of these samples were conducted using a Hitachi S-3400N scanning electron microscope (SEM) at Qingdao Institute of Marine Geology.

The radiogenic Sr and Nd isotopic compositions of the wet sieved <63 μm siliciclastic fractions were measured on eighteen samples from Core CSDP-1 and one sample from the paleo-Yangtze River sediment in Nanjing. This fine-grained fraction was used to minimize the grain-size effect on Sr isotope compositions (e.g., Jonell et al., 2018; Yang et al., 2007a; Zhao et al., 2017). The terrigenous materials were chemically extracted using the same procedure as for the clay minerals analysis. About 200 mg powdered samples were then weighted and dissolved in Savillex vials (15 ml teflon) in a mixture of ultrapure HF (24 mol/L), HNO_3 (14 mol/L) and $HClO_4$ (12 mol/L) for four days at 160 °C on a hotplate. The material was then evaporated to dryness and the samples were dissolved in aqua regia and heated for 24 h at 130 °C. Sr and Nd were separated using standard ion exchange techniques (Révillon et al., 2011). In this study, the Sr and Nd isotopic compositions were measured in static mode on a Thermo TRITON thermal ionization mass spectrometer (TIMS) at the PSO (Pôle de Spectrométrie Océan) in Brest, France. Additional Sr and Nd isotopes of one sample from the paleo-Yangtze River were measured using a Thermo TRITON and a Neptune plus multicollector inductively coupled plasma-mass spectrometer (MC-ICPMS), respectively, at the State Key Laboratory for Mineral Deposits Research, Nanjing University. All measured Sr and Nd ratios were normalized to $^{86}Sr/^{88}Sr = 0.1194$ and $^{146}Nd/^{144}Nd = 0.7219$, respectively. During the measurement period, the result obtained on the NBS987 Sr standard solution was $^{87}Sr/^{86}Sr = 0.710254 \pm 0.000005$, and the JNdi Nd standard solution was $^{143}Nd/^{144}Nd = 0.512103 \pm 0.000003$. Nd isotopic data are reported as: $\varepsilon Nd = [((^{143}Nd/^{144}Nd)_{sample}/0.512638)-1] \times 10^4$ (Jacobsen and Wasserburg, 1980). Sr and Nd concentrations and isotopic ratios measured on the fine-grained siliciclastic fraction (< 63 μm) from Core CSDP-1 are showed in Table 2.

4. Results

4.1. Grain-size and mass accumulation rates (MAR)

In general, mean grain-size of terrigenous materials at Core CSDP-1 shows a sharp decrease since about 0.8 Ma (Fig. 2). Specifically, the terrigenous grain size of sediments deposited between 3.5 and 0.8 Ma varies between 6.4 and 507.0 μm with an average of 92.1 μm. In contrast, the mean grain size of terrigenous sediments since 0.8 Ma is finer and varies between 7.3 and 97.0 μm, with an

Table 1
Clay mineral assemblages of Core CSDP-1 and potential source areas.

Sample ID	Samples Sites		Smectite (%)	Illite (%)	Kaolinite (%)	Chlorite (%)	Illite chemical index	Illite crystallinity (Δ2θ)	Smectite crystallinity (Δ2θ)
	CSDP-1	average (0–300 m) n = 162	34	49	7	10	0.42	0.27	1.33
		average (0–82 m) n = 47	25	61	6	8	0.36	0.33	1.41
		average (82–300 m) n = 115	38	45	7	10	0.44	0.24	1.30
YR-1	Guide	surface sample/Clayey Silt	11	69	7	13	0.34	0.26	1.20
YR-2	Lanzhou	surface sample/Clayey Silt	19	64	6	10	0.33	0.37	0.74
YR-3	Qingtongxia	surface sample/Clayey Silt	19	60	7	14	0.36	0.29	0.86
YR-4	Zhaojunfen	surface sample/Clayey Silt	16	67	5	12	0.40	0.36	0.86
YR-5	Jundu	surface sample/Clayey Silt	39	44	6	11	0.34	0.28	0.59
YR-6	Songjiachuan	surface sample/Clayey Silt	41	44	6	9	0.34	0.35	0.78
YR-7	Tongguan	surface sample/Silt	33	49	8	9	0.27	0.35	0.78
YR-9	Huayuankou	surface sample/Clayey Silt	22	59	9	10	0.33	0.35	1.03
YR-14	Huayuankou	surface sample/Clayey Silt	29	54	8	9	0.37	0.34	1.09
YR-12	Pingyin	surface sample/Clayey Silt	26	55	7	11	0.35	0.31	0.87
YR-15	Pingyin	surface sample/Clayey Silt	23	58	9	10	0.31	0.30	0.95
YR-16	Pingyin	surface sample/Clayey Silt	38	45	8	9	0.34	0.37	0.72
YR-11	Beizhen	surface sample/Clayey Silt	31	52	7	9	0.30	0.34	1.11
YR-13	Lijin	surface sample/Clayey Silt	40	44	8	9	0.29	0.33	0.65
YR-10	Kenli	surface sample/Clayey Silt	34	50	7	9	0.35	0.32	0.79
YR-17	Kenli	surface sample/Clayey Silt	44	39	8	9	0.29	0.29	0.62
N4-1	Nanjing baguazhou	surface sample/Silty Clay	22	53	17	9	0.70	0.28	0.87
N4-2	Nanjing baguazhou	surface sample/Silty Clay	19	54	14	13	0.69	0.26	0.86
Paleo-Yangtze River Nanjing Guizishan		Pliocene-middle Pleistocene/Conglomerate and thick-bedded pebbly Sandstone	81	8	11	0	0.53	0.35	0.76
Loess11	Lingtai Loess	34 ka/Clayey Silt	11	68	6	14	0.30	0.28	1.18
Loess124	Lingtai Loess	889 ka/Clayey Silt	32	62	4	2	0.34	0.27	1.25
Loess172	Lingtai Loess	1252 ka/Clayey Silt	15	76	5	3	0.30	0.26	0.78
Loess330	Lingtai Loess	2603 ka/Clayey Silt	39	44	8	9	0.36	0.27	1.15
Loess400	Lingtai Loess	3665 ka/Clayey Silt	29	56	6	9	0.26	0.35	1.62
Yellow River		average n = 16	29 (11–44)	54 (39–69)	7 (5–9)	10 (9–14)	0.33	0.33	0.85
Yangtze River		average n = 2	20 (19–22)	54 (53–54)	15 (14–17)	11 (9–13)	0.70	0.27	0.87
Lingtai Loess		average n = 5	25 (11–39)	61 (44–76)	6 (4–8)	8 (2–14)	0.31	0.29	1.20
Core PD (modern Yangtze delta)[a]		Late Pliocene-middle Pleistocene average n = 38	39 (2–100)	46 (0–85)	9 (0–24)	7 (0–21)	\	\	\
Yalu River[b]		average n = 2	2 (1–3)	68 (64–72)	12 (11–14)	18 (15–20)	\	\	\
Taedong & Chongchon Rivers[c]		average n = 1	4	70	12	14	\	\	\
Han River[d]		average n = 14	2	60	17	21	\	\	\
Geum River[d]		average n = 9	1	55	21	24	\	\	\
Geum River[b]		average n = 1	4	60	19	17	\	\	\
Yeongsan River[d]		average n = 3	2	64	15	20	\	\	\

Note: "\" indicates no data.
[a] Data from Chen et al. (2014).
[b] Data from Yang et al. (2003b).
[c] Data from Li et al. (2014b).
[d] Data from Cho et al. (2015); All published clay mineral data cited in this study have been recalculated by the method of Biscaye (1965).

average of 33.4 μm. Grain-size distributions of the four representative samples from different sedimentary facies (floodplain, river channel and coastal deposit) (Fig. 2) show bimodal/trimodal patterns, with two or three modal grain sizes near 1.8 μm, 10 μm, 50 μm and 250 μm. The coarsest component with a modal size of >200 μm mainly appears below ~82 m (>0.8 Ma).

Total MAR in Core CSDP-1 varies in the range of 10.3–45.1 g/cm^2/ky, with an average of 21.1 g/cm^2/ky. In general, total MAR is very low and stable between 3.5 and 0.8 Ma and rapidly increases after ~0.8 Ma (Fig. 3).

4.2. Clay mineralogy

Results of clay mineral assemblages are shown in Figs. 3–5 and Table 1. The assemblages mainly consist of illite (13–79%, average 49%) and smectite (7–81%, average 34%). Chlorite (1–20%) and kaolinite (1–18%) are present in lesser amounts, with average contents of 10% and 7%, respectively. On the long-term timescale, smectite, kaolinite and chlorite gradually decreased since 3.5 Ma, while illite increased. From about 3.5 Ma to 0.8 Ma, illite (average 45%) and smectite (average 38%) were the dominant components, with associated chlorite (average 10%) and kaolinite (average 7%), characterized by overall high-frequency variability. In contrast, the illite content rapidly increased to about 61% after ~0.8 Ma, while the smectite content decreased to ~25%, and is characterized by small fluctuations. The illite chemical index varies between 0.26 and 0.66, with an average of 0.42, suggesting that the illite is rich in Fe-Mg, and was formed by strong physical weathering and weak chemical weathering (Esquevin, 1969). The crystallinities of smectite and illite vary between 0.41 and 1.87°Δ2θ and 0.19–0.41° Δ2θ, with

Table 2
Sr-Nd isotopic composition of Core CSDP-1 since 3.5 Ma and potential sources areas.

Sample ID	Age (Ma)	Sr (μg/g)	Nd (μg/g)	$^{87}Sr/^{86}Sr$ ($\pm2\sigma \times 10^{-6}$)	$^{143}Nd/^{144}Nd$ ($\pm2\sigma \times 10^{-6}$)	εNd ($\pm2\sigma$)
U1	0.03	180.3	20.5	0.716833 ± 6	0.512019 ± 4	−12.1 ± 0.08
U2	0.19	100.5	30.2	0.722498 ± 6	0.512073 ± 6	−11.0 ± 0.12
U3	0.36	124.8	27.7	0.721218 ± 6	0.512017 ± 15	−12.1 ± 0.29
U4	0.52	201.3	25.2	0.715734 ± 5	0.511987 ± 4	−12.7 ± 0.08
U5	0.69	166.7	28.7	0.718752 ± 5	0.512000 ± 8	−12.4 ± 0.16
U6	0.82	116.5	30.7	0.721382 ± 6	0.512040 ± 9	−11.7 ± 0.18
U7	0.92	161.4	17.3	0.715281 ± 5	0.512146 ± 7	−9.6 ± 0.14
U8	1.02	148.0	24.3	0.717376 ± 7	0.512089 ± 4	−10.7 ± 0.08
U9	1.27	175.6	19.8	0.713853 ± 7	0.512137 ± 8	−9.8 ± 0.16
U10	1.55	140.2	16.8	0.717485 ± 5	0.512126 ± 7	−10.0 ± 0.14
U11	1.82	149.3	23.9	0.714999 ± 6	0.512142 ± 9	−9.7 ± 0.18
U12	2.00	149.7	13.9	0.715422 ± 6	0.512109 ± 6	−10.3 ± 0.12
U13	2.16	141.2	21.5	0.716578 ± 5	0.512107 ± 5	−10.4 ± 0.10
U14	2.31	109.8	18.5	0.719247 ± 6	0.512120 ± 8	−10.1 ± 0.16
U15	2.46	152.6	20.1	0.714761 ± 5	0.512167 ± 6	−9.2 ± 0.12
U16	2.64	91.6	31.1	0.727355 ± 5	0.512080 ± 9	−10.9 ± 0.18
U17	2.90	64.3	37.3	0.723713 ± 6	0.512055 ± 7	−11.4 ± 0.14
U18	3.14	124.6	21.8	0.716841 ± 7	0.512203 ± 339	−8.5 ± 0.40
average (82-0 m) (n = 6)		148.4	27.2	0.719403 ± 6	0.512023 ± 8	−12.0 ± 0.15
average (300-82 m) (n = 12)		134.0	22.2	0.717743 ± 6	0.512124 ± 35	−10.0 ± 0.16
Paleo-Yangtze River (Plio-mid Pleistocene)		\	\	0.724708 ± 8	0.512065 ± 4	−11.2 ± 0.08
Yellow River[a] (n = 15)				0.719505 ± 14	0.511994 ± 10	−12.6
Yangtze River[b] (n = 15)				0.722420 ± 8	0.512060 ± 9	−11.3

[a] Data from Hu et al. (2012).
[b] Data from Yang et al. (2007a).

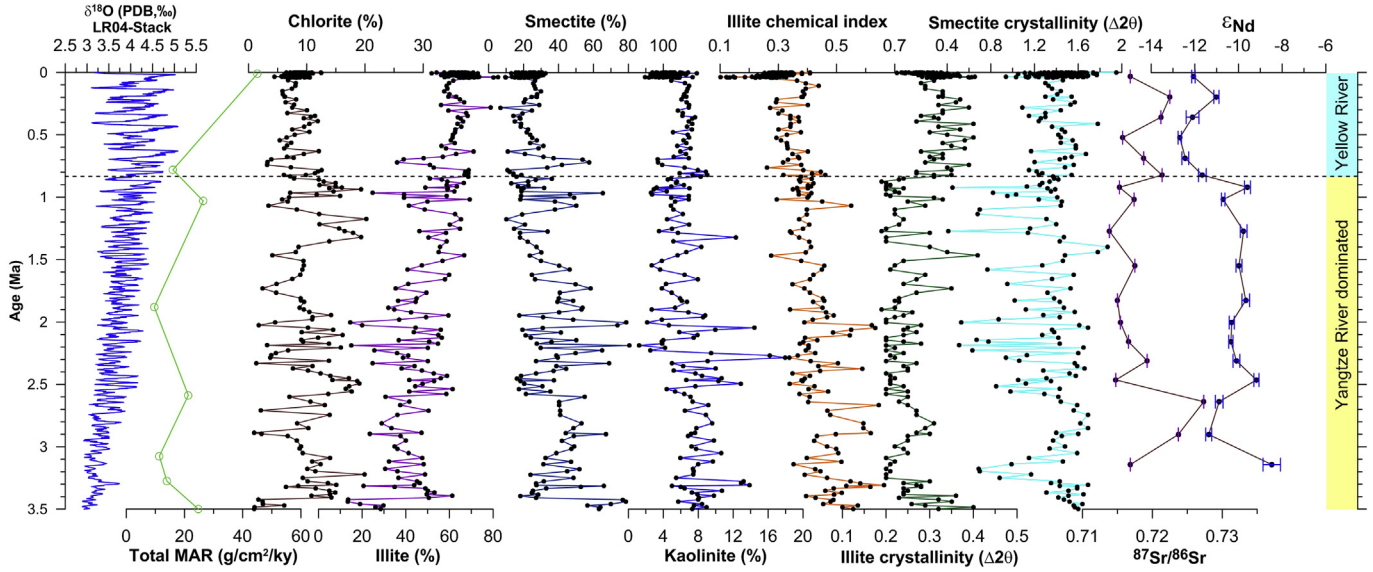

Fig. 3. Comparison of total mass accumulation rate (MAR), clay minerals assemblages, illite chemical index, crystallinity index, $^{87}Sr/^{86}Sr$, εNd in CSDP-1 and global climate change as indicated by deep-sea $\delta^{18}O$ LR04-Stack (Lisiecki and Raymo, 2005) since 3.5 Ma. Horizontal dashed black line across all frames around 82 m indicates the boundary of provenance transition. The blue and yellow shades represent the provenance dominated by the Yellow and Yangtze Rivers, respectively. (For interpretation of the references to colour in this figure legend, the reader is referred to the Web version of this article.)

average values of 1.33° and 0.27° $\Delta2\theta$, respectively. As with the downcore variations of clay mineral assemblages, both illite and smectite crystallinity index display a clear increase especially since 0.8 Ma, while illite chemical index decreased (Fig. 3).

The high-resolution variations of clay minerals of Core CSDP-1 since about 42 ky B.P. are shown in Fig. 4 and Table 1. The assemblages mainly consist of illite (56–82%, average 66%) and smectite (10–31%, average 21%). Chlorite (4–13%) and kaolinite (2–7%) are present in lesser amounts, with average contents of 8% and 5%, respectively. In general, the clay mineral assemblage remains relatively stable since the last glaciation, but still displays slightly (<2%) higher contents of illite and lower smectite, kaolinite and chlorite during the last glaciation than the Holocene.

Clay minerals in the lower reaches of Yangtze River consist mainly of illite (average 54%) and smectite (average 20%), with lower amounts of kaolinite (average 15%) and chlorite (average 11%). In contrast, the clay mineral assemblages of the Yellow River consist of illite (average 54%), smectite (average 29%), chlorite (average 10%) and kaolinite (average 7%), characterized by higher contents of smectite compared to the Yangtze River. Moreover, the paleo-Yangtze River sediment at Nanjing has very high smectite contents (81%). As with the Yellow River sediment, the clay mineral

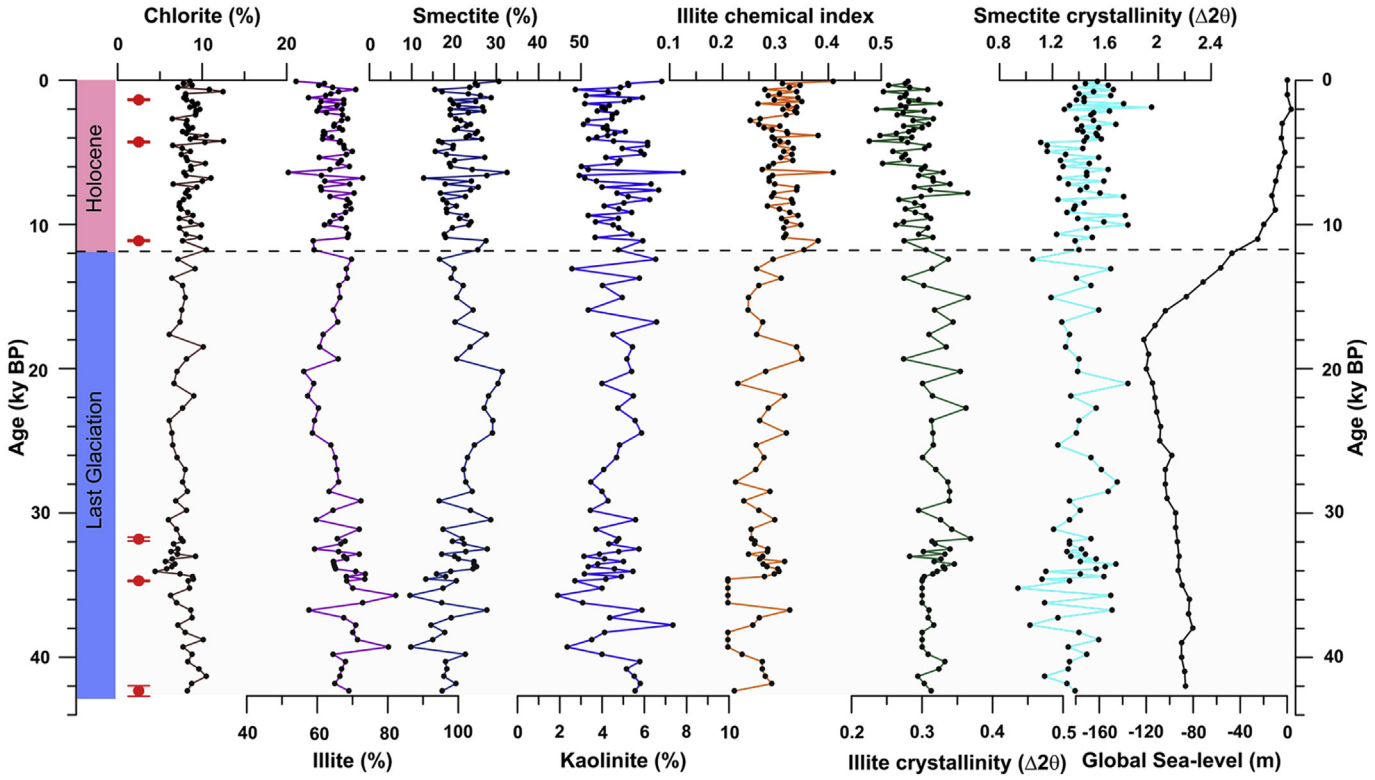

Fig. 4. The high-resolution variation of clay minerals assemblages, illite chemical index, crystallinity index and global sea-level record (Miller et al., 2005) since about 42 ky B.P. The dash lines show the boundaries of last glacial and Holocene and red dots show 6 Accelerator Mass Spectrometry (AMS) ^{14}C dates (Liu et al., 2018). (For interpretation of the references to colour in this figure legend, the reader is referred to the Web version of this article.)

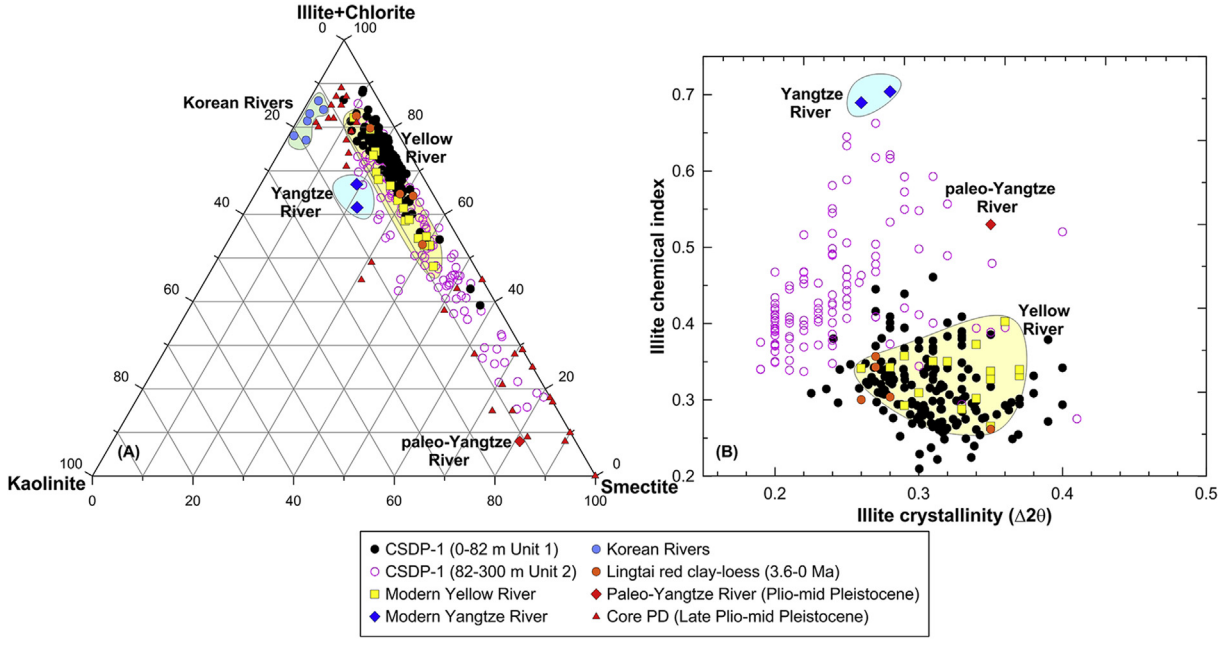

Fig. 5. Provenance discrimination plot of clay minerals. (A) A ternary diagram of smectite-(illite + chlorite)-kaolinite and (B) a diagram of illite crystallinity vs. illite chemical index. It shows the clay mineral composition of sediments from Core CSDP-1 (Units 1 and 2) and their potential sources, including the Lingtai red clay-loess (3.6–0 Ma), modern Yellow River, modern Yangtze River, paleo-Yangtze River (formed during the Pliocene-middle Pleistocene), PD Core (formed during the late Pliocene-middle Pleistocene) in the modern Yangtze delta (Chen et al., 2014) and Korean Rivers (Cho et al., 2015; Li et al., 2014b; Yang et al., 2003b). (For interpretation of the references to colour in this figure legend, the reader is referred to the Web version of this article.)

assemblages of loess samples are relatively high in smectite content with an average of 25% (Fig. 5 and Table 1).

4.3. Sr-Nd isotopes

Sr and Nd concentrations of Core CSDP-1 samples vary between 64.3 and 201.3 μg/g and 13.9 and 37.3 μg/g, respectively. The $^{87}Sr/^{86}Sr$ ratio displays a wide range between 0.713853 and 0.727355 and the εNd ranges between −12.7 and −8.5 with an average of −10.7, as shown in Figs. 3 and 6. In general, εNd values show a relatively stable trend from about 3.5 to 0.8 Ma and become more negative since ~0.8 Ma (Fig. 3). The $^{87}Sr/^{86}Sr$ ratio and εNd value of the paleo-Yangtze River sample are 0.724708 and −11.2, respectively (Table 2 and Fig. 6).

4.4. Microscope observation

The microscopic examinations show that opaque minerals, such as magnetite and ilmenite, were more abundant at 3.5–0.8 Ma, but reduced in importance after 0.8 Ma. Representative plane-polarized microscope images of bulk samples and SEM images of clay-sized fraction of sediment deposited at ~0.52 Ma and ~1.55 Ma are shown in Fig. 7. The morphological examinations of 45 SEM images demonstrate that clay minerals are characterized by detrital flakes, platy particles, angular borders and typically irregular shapes (Fig. 7C and D). This suggests a terrigenous origin, insignificant pedogenesis and diagenesis of clay minerals in Core CSDP-1.

5. Discussion

5.1. Large-scale transgression in the Yellow Sea

The core section is divided into two major lithologic units (Units 1 and 2), distinguished on the basis of microfossil assemblages (Liu et al., 2018), grain-size and visual core description (i.e., sediment composition, sedimentary texture and structure). The determination of sedimentary facies (terrestrial and marine facies) is particularly based on the abundance of shallow-water marine species (foraminifera and marine ostracods) relative to shallow-water euryhaline species (Liu et al., 2018) (Fig. 2E and F). The upper ~82 m (~0.8 Ma) of the studied core (Unit 1) is composed of gray to dark gray clayey silt or silt with shallow marine species (foraminifera and marine ostracods), intercalated with a few thin, fine-sand beds. Silty bandings and bivalves shells are widespread throughout this unit, and shallow marine species (foraminifera and marine ostracods) are abundant, indicative of dominant marine deposition. Unit 1 is further divided into three subunits from top to bottom based on sediment grain-size, structure and composition. These are interpreted as dominantly tidal-dominated coastal deposits (1a), a delta deposit (1b) and a coastal deposit (1c), respectively. In contrast, the lower section (Unit 2) (82–300 m, ~0.8–3.5 Ma) is dominated by grayish yellow to dark brown sand or sandy silt, interbedded with several silt beds and a few gravel layers. In this unit, cross bedding, plant fragments, brown rusty stains and calcium nodules are common, with few bivalves shells or shallow-water marine species (foraminifera and marine ostracods). These characteristics are interpreted to indicate a dominantly nearshore terrestrial environment. Similarly, Unit 2 is further subdivided into an alternation of river channels deposits (2a), river floodplain/lacustrine deposits (2b), river channels deposits (2c) and river floodplain/lacustrine deposits (2d) (Fig. 2A–H).

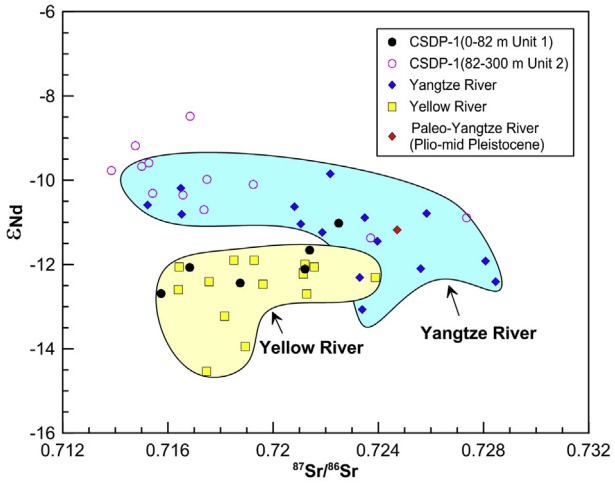

Fig. 6. Sediment provenance discrimination diagram of Sr-Nd isotopes. For comparison, the Sr and Nd isotope data of sediments from the Yangtze River (Yang et al., 2007a) and Yellow River (Hu et al., 2012).

The dominant fluvial/lacustrine deposits of Unit 2 and coastal/delta deposits of Unit 1 suggest that a terrestrial environment prevailed in the study area from ~3.5 to 0.8 Ma (300–82 m) and then shifted to a shallow marine sedimentary environment after about 0.8 Ma. Another three thin sediment layers (<5 m thick) with a few marine species (foraminifera and marine ostracods) at depths of around 112 m (~1.03 Ma), 135 m (~1.44 Ma), and 145 m (~1.66 Ma) were identified below 82 m (Liu et al., 2016a, 2018) (Fig. 2E and F), suggesting a few transient (<40 ky) marine transgressions during accumulation of the late Pliocene and mid-Pleistocene fluvial deposits. In general, regional comparison of the large-scale transgression sequences of a series of long drilling cores, including Core CSDP-1 (this study), Core QC2 (Zhou and Ge, 1990), Core NHH01 (Liu et al., 2014) in the central Yellow Sea and Core BH08 (Yao et al., 2017) in the central Bohai Sea, shows that the onset of large-scale transgression in the Yellow and Bohai Seas during the Quaternary is roughly synchronous and occurred consistently since ~0.8 Ma (Fig. 8A–D). In contrast, the boreholes from the modern Yangtze and Yellow Rivers deltas suggested that the fluvial deposit dominated there during the late Pliocene-late Pleistocene and foraminifera occurrence only became more common since the late Pleistocene, possibly because of combined influence of local geomorphology change and regional transgression (e.g., Chen et al., 2014; Liu et al., 2016b; Yang et al., 2001; Yi et al., 2016; Yue et al., 2018).

Because of the growth of the Northern Hemisphere ice sheets, global sea-level experienced a gradual and long-term drop since the late Pliocene, which was superposed by large amplitude sea-level fluctuations (>100 m) on glacial-interglacial cycles with major periods of 40 ky before mid-Pleistocene transition (MPT) and 100 ky thereafter (Miller et al., 2005) (Fig. 8H). However, the obvious cyclic alternation of lithology between land and marine facies in the Yellow Sea was absent between 3.5 and 0.8 Ma and only occurred after 0.8 Ma (Fig. 2). That means that the sedimentary environment in the Yellow Sea since the late Pliocene was almost not influenced by global sea-level change until 0.8 Ma. Although sediment deposited on the continental shelf is possibly not continuous because of erosion during glacial lowstands (Hanebuth et al., 2011), however, there is no reason why this shelf erosion process would preferentially affect sediments between 3.5 and 0.8 Ma, during which amplitude of sea-level change was much smaller than that since 0.8 Ma. Systematic rock magnetic analyses and AMS ^{14}C dating also suggested no significant sedimentation hiatus in the Core CSDP-1 (Liu et al., 2016a, 2018). Therefore, we propose that there was likely a topographic barrier preventing the

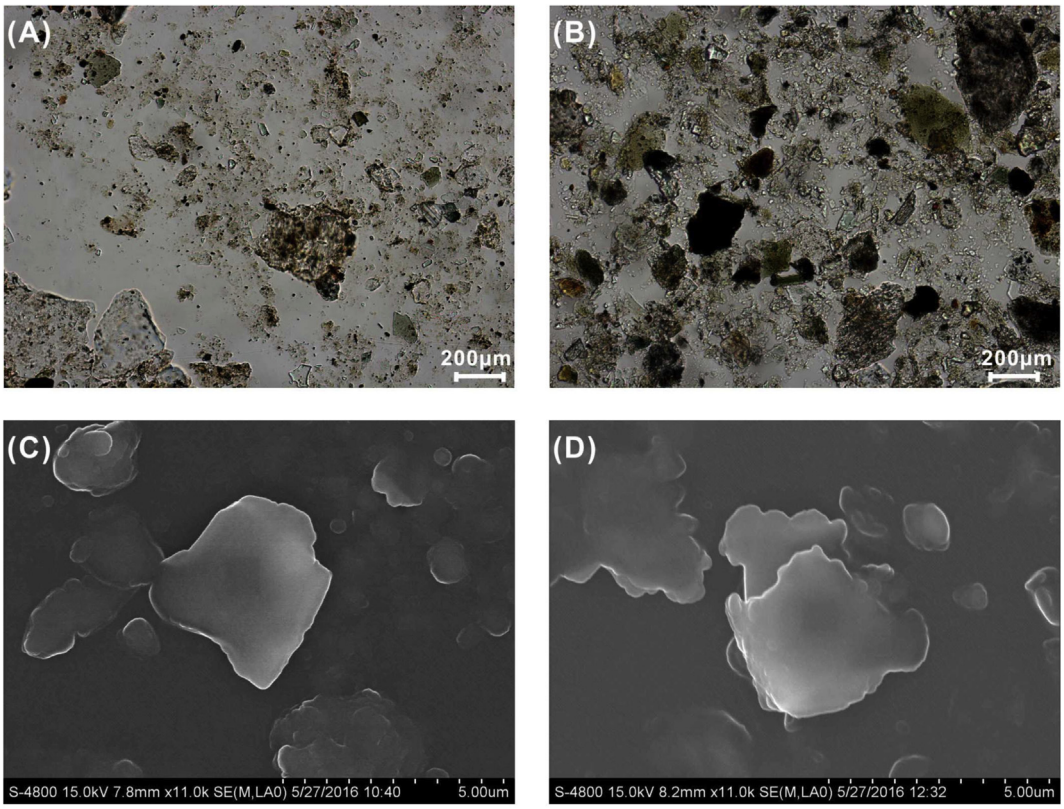

Fig. 7. Representative plane-polarized microscope images of bulk samples (A and B) and scanning electron micrographs (SEM) images of clay minerals (C and D). Sample CS55-08 (A and C) deposited at 50 m at ~0.52 Ma and sample CS156-06 (B and D) deposited at 140 m at ~1.55 Ma.

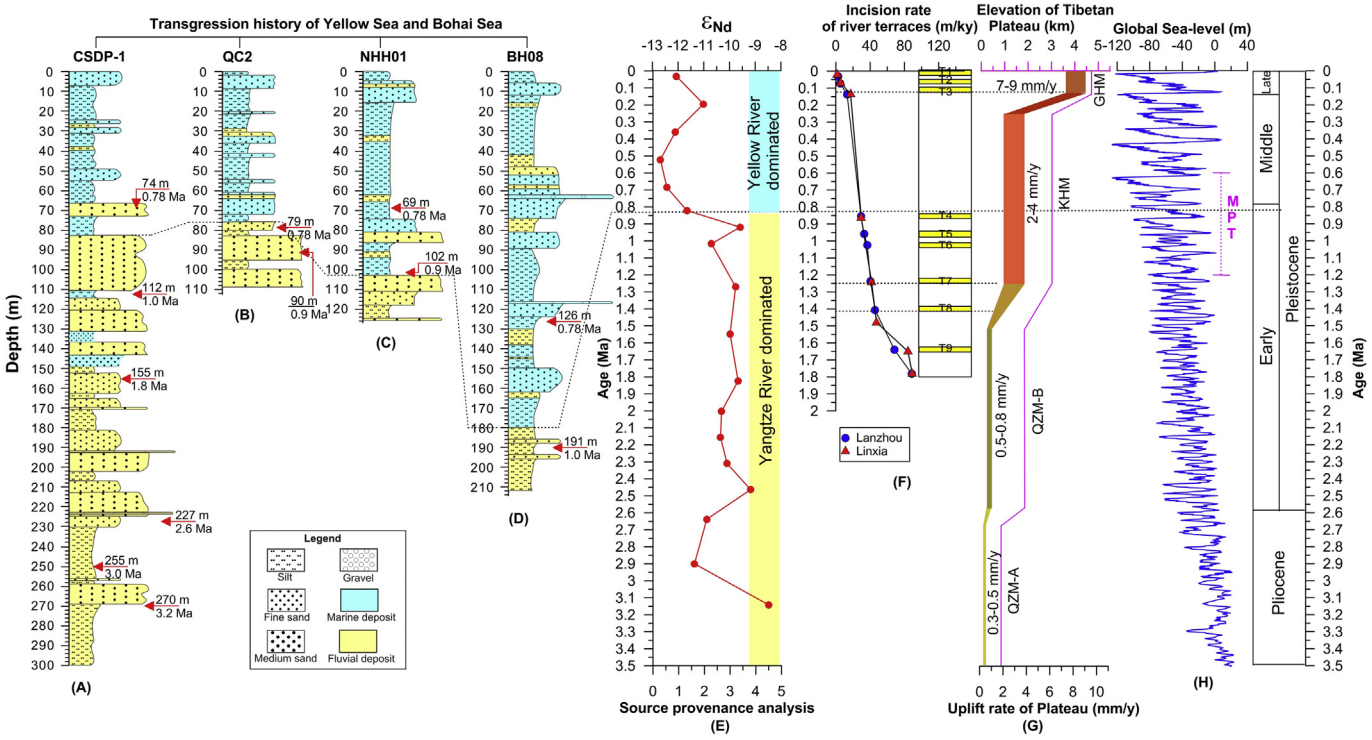

Fig. 8. Correlation of (A–D) transgression history of Yellow Sea (core CSDP-1 (this study), QC2 (Zhou and Ge, 1990) and NHH01 (Liu et al., 2014)) and Bohai Sea (core BH08 (Yao et al., 2017)), (E) source provenance analysis, (F) incision rate of Yellow river terraces (Li et al., 2014a), (G) uplift of Tibetan Plateau (Gu, 2015; Li et al., 2014a), and (H) global sea-level record (Miller et al., 2005). The red arrow indicates the age control points. (For interpretation of the references to colour in this figure legend, the reader is referred to the Web version of this article.)

intrusion of seawater from the East China Sea to the Yellow and Bohai Seas before ~0.8 Ma. Previous studies showed that these marine transgressions in the Yellow Sea and around this region were possibly controlled by tectonic subsidence of the Min-Zhe Uplift (Liu et al., 2016a, 2018; Yi et al., 2014; Zhao et al., 2019). Large scale volcanic eruptions in the late Mesozoic are associated with uplift of the Min-Zhe Uplift that became a barrier between East Asia and the Pacific Ocean (Qin et al., 1989; Yi et al., 2014). The Min-Zhe Uplift gradually crushed and eroded since the early Cenozoic and subsided below sea-level in the early Quaternary, allowing the large scale marine transgression sediments to be deposited in this area, although the exact time of this connection was unclear (Qin et al., 1989; Yi et al., 2014; Zhao et al., 2019). Our study demonstrates that tectonic subsidence of the Min-Zhe Uplift was the first-order control on the evolution of sedimentary environments in the Yellow and Bohai Seas and large-scale transgression of the Yellow and Bohai Seas occurred since the middle Pleistocene.

5.2. Potential sediment sources

The interpretation of the terrestrial mineralogical and geochemical records requires detailed knowledge of the potential source areas, as well as the mode, strength and history of the transport processes involved (e.g., Shen et al., 2017; Yang et al., 2003b). We emphasize that this study focuses on provenance change on the tectonic timescale (million years) rather than short timescale (i.e., glacial-interglacial or less). In the case of almost no any information about the variations in sediment flux of the potential rivers through the studied time interval, the simple assumption is that the modern sediment flux of the potential sources can be taken as the reference for their comparison in the geological past to some extent. The modern Yellow and Yangtze Rivers respectively deliver 1100 Mt and 470 Mt of suspended sediments annually to the East Asian marginal seas (Milliman and Farnsworth, 2011), while the sediment fluxes of the two rivers before 2000 years ago were suggested to be only about 20% of the present level because of the less influence of human activities (Saito et al., 2001; Wang et al., 2011). At present, the sediments in the western South Yellow Sea are mainly supplied by the Yellow River (Lu et al., 2015; Qin et al., 1989; Yang et al., 2003b), with minor delivery from the Yangtze River (Wei et al., 2001) based on mineralogical and geochemical evidence. Other potential sources are small localized rivers, such as Huai, Hai, Luan and Liao Rivers etc (Fig. 1). However, their contribution to the study area is probably minor because of relatively low suspended sediment flux in total (~76 Mt/yr) from these rivers (Milliman and Farnsworth, 2011). In addition, the main rivers (i.e., the Yalu, Chongchon, Taedong, Han, Geum and Yeongsan Rivers) (Fig. 1) originating in the Korean Peninsula deliver about 18 Mt/yr of suspended sediments to the eastern Yellow Sea (Milliman and Farnsworth, 2011), however, the supply of Korean river sediments to the western South Yellow Sea is likely also negligible because of the low sediment discharge (Yang et al., 2003b). Moreover, the influence of modern eolian dust to South Yellow Sea sedimentation can be neglected because of dilution by the huge sediment fluxes from the Yellow and Yangtze Rivers (Qiao et al., 2017). This dust contribution would become less important before the middle Pleistocene, as revealed from decreased eolian flux on both the Loess Plateau (Sun and An, 2005) and the northern South China Sea (Wan et al., 2007).

Although it is clear that at present the study area is dominated by sediment supply from the Yellow River (Lu and Li, 2015; Qin et al., 1989; Yang et al., 2003b), the sediment source possibly changed since the Pliocene as some studies suggest that the paleo-Yellow River likely began draining through the North China Plain and modern Yellow River delta since the middle Pleistocene (Yang et al., 2001) and the paleo-Yangtze River possibly flowed into the South Yellow Sea before the middle Pleistocene (Chen and Stanley, 1995; Li et al., 2011a). In any case, it seems reasonable that the main potential sediment sources of the study core since the late Pliocene are the paleo-Yangtze and/or paleo-Yellow Rivers.

In order to better constrain the provenance we also have to take into account the possible sediment source change of the paleo-Yangtze or paleo-Yellow Rivers over the study period, although this is difficult because of scarcity of data. The Yellow and Yangtze drainage basins have completely different geologic and climatic conditions (Yang et al., 2004). The Yellow River is located on the old Archean North China Craton (Yang et al., 2004). Approximately 90% of Yellow River sediment derives from the Loess Plateau in the middle reaches (Ren and Shi, 1986), and it largely inherits the loess characteristics (Yang et al., 2001), in being particularly rich in smectite and carbonate (Fan et al., 2001). Thus, long-term variations in the provenance of the Yellow River should basically reflect changing loess composition (Li et al., 2011b). Through the Quaternary, the provenance of sediment in the Chinese loess/deserts has not significantly changed, at least as revealed by both Sr–Nd isotope compositions (Chen and Li, 2013) and clay mineral assemblages (Gylesjö and Arnold, 2006). Our study on Lingtai red clay-loess sequence demonstrates the relatively stable character of the clay mineral assemblages since the late Pliocene (Table 1 and Fig. 5), which is similar to modern Yellow River clay mineralogy. Consequently, the sediment derived from the Yellow River would be expected to yield no significant change in provenance since the late Pliocene (Yang et al., 2001).

In contrast, the Yangtze River basin is located on the Yangtze Craton and South China orogen (Yang et al., 2004). The upper reaches of the Yangtze River are marked by metamorphic rocks, carbonate rocks and Mesozoic clastic rocks and igneous rocks; in contrast, the middle-lower reaches are typified by acidic-metamorphic bedrocks and Quaternary sediments (Yang et al., 2007a). Yangtze River sediment is dominantly derived from the upper reaches, especially from the four major tributaries (Jinsha River, Min River, Jialing River and Wu River) in the headwater, because of high relief and abundant monsoon rainfall (Yang et al., 2006b). The Nd isotopic and rare earth element (REE) compositions of sediment from a core (PD-99) drilled in the modern Yangtze River delta suggest a generally stable sediment source since the Pliocene (Yang et al., 2007b) (Fig. 1). The paleo-Yangtze River sediment in the lower reaches (e.g., Nanjing region) is characterized by a suite of thick-bedded gravel sediments, known as the Yuhuatai Gravel Bed formed since the Miocene (Zheng et al., 2013). Recent studies proposed that Yuhuatai Gravel Bed can be divided into four formations (i.e., the Dongxuanguan Formation, the Luhe Formation, the Huanggang Formation, and the Yuhuatai Formation) and Han et al. (2009) inferred that the Yuhuatai Formation was deposited between the Pliocene and middle Pleistocene and overlaid by the Xiashu Loess. In this study, we analyzed the Sr-Nd isotopic composition of a sample from the Yuhuatai Formation in Nanjing. As shown in Table 2 and Fig. 6, the Sr-Nd isotopic compositions of sediment from pre-mid-Pleistocene Yangtze River in Nanjing fall in the range of the modern Yangtze River, confirming the stable provenance of Yangtze River since the late Pliocene (Yang et al., 2007b).

However, we note that there is a remarkable difference in clay mineralogy between the Pliocene to mid-Pleistocene and the modern Yangtze River (Table 1 and Fig. 5). The clay mineral assemblage of sediment from the Yuhuatai Formation shows dominance of smectite (81%) with minor kaolinite (11%) and illite (8%) (Table 1 and Fig. 5). Remarkable, previous clay minerals studies

on the paleo-river/lacustrine sediment from the lower reaches in Nanjing (Li et al., 2011b) and modern delta (Chen et al., 2014) of Yangtze River also indicate that the paleo-Yangtze River sediment during the late Pliocene and mid-Pleistocene is rich in smectite (Table 1 and Fig. 5).

Some of previous studies suggested that the paleo-Yangtze River changed its drainage basin from a local small one to a large river originating on the eastern Tibetan Plateau during the early Pleistocene (Yang et al., 2006a). At that time, the river sediment was mainly eroded from the local Bailonggang basalt when the modern delta region stood as uplands rather than low relief (Chen et al., 2014; Yue et al., 2018). The weathering of such basalt bedrock would supply sediment with high smectite content. However, the dramatic change in sediment source of Yangtze River since the late Pliocene is not supported by trace elements and Nd isotope composition (Yang et al., 2007b and this study). Here, we prefer to another interpretation about the discrepancy between clay minerals and Nd isotopes. The chemical weathering of basaltic rocks in wet and humid regions can produce abundant of smectite (Chamley, 1989). Especially, the middle to late Permian basic rock (Emeishan large igneous province) is widely distributed in the upper Yangtze basin with an area of $>2.5 \times 10^5$ km^2 (Chung and Jahn, 1995). The weathering of basaltic rock is strongly dependent on temperature (Li et al., 2016) and has several times higher weathering rate than other silicate rocks (i.e., granitoids and metamorphics) (Dessert et al., 2003; Schopka et al., 2011). Therefore, it is expected that ~5 °C higher temperature and stronger monsoon precipitation during the late Pliocene than the late Pleistocene (Sun and An, 2005; Wan et al., 2007) would accelerate the weathering of rocks, especially the abundant basaltic rocks and other basic rocks (i.e., Emeishan and Bailonggang basalt) in the Yangtze River drainage basin into smectite even the major provenance remains unchanged. This mechanism well explains the higher smectite content and invariable εNd value of paleo-Yangtze River sediment before the mid-Pleistocene in comparison with modern river sediment. Nd isotopic variations of the late Cenozoic sediments in Jianghan Basin (Fig. 1), a major sediment depocenter at the middle Yangtze River, also suggested a stable sediment source since at least the late Pliocene (Shao et al., 2012). Unfortunately, there is no available data of clay minerals from the Jianghan Basin to verify whether the Pliocene-middle Pleistocene sediments deposited there are also dominated by smectite. Although the origin of smectite of paleo-Yangtze River sediments remains a mystery, it's no doubt that the Yangtze River appears to develop into a large river similar as the modern Yangtze no later than the late Pliocene (Shao et al., 2012; Yang et al., 2007b).

5.3. Clay mineral and Sr-Nd isotope constraints on provenance

In order to discriminate the sources of clay minerals at Core CSDP-1, we plot diagrams of smectite-(illite + chlorite)-kaolinite and illite crystallinity vs. illite chemical index (Fig. 5). Clay mineral assemblages of two units at CSDP-1 deviate from the Korean rivers and modern Yangtze River patterns, and are subparallel to the (illite + chlorite)-smectite line. Almost all samples of Unit 1 (82–0 m) are very similar to the modern Yellow River and Lingtai red clay-loess, and plot as a group. In contrast, Unit 2 (82–300 m) sediments plot between modern Yellow River/Lingtai red clay-loess sediment and paleo-Yangtze River sediment (Fig. 5A). This trend can be interpreted to mean that Unit 2 was primarily sourced from the paleo-Yangtze River (high smectite end-member), and Unit 1 is from the Yellow River sediment (high illite-chlorite end-member). The illite crystallinity vs. illite chemical index plot (Fig. 5B) further demonstrates that almost all Unit 1 samples overlap with sediment from the Yellow River/Lingtai red clay-loess, characterized by more Fe-Mg-rich illite, while Unit 2 samples partly overlap with the Pliocene-mid Pleistocene paleo-Yangtze River sediment, characterized by more Al-rich illite. As the major sediment supplier of the Yellow River, loess deposits of the Chinese Loess Plateau display no significant long-term variation of clay minerals (Gylesjö and Arnold, 2006 and this study) or Nd isotopic compositions (Chen and Li, 2013), excluding changes in sediment composition of the Yellow River itself as a possible reason of distinct variation in clay mineralogy at the study core at 0.8 Ma.

In addition to provenance change, other offshore processes may also influence the clay mineral assemblage of the core sediment in continental margin, such as hydraulic sorting, as well as diagenesis and/or pedogenesis after burial (Chamley, 1989). The possible segregation of clay minerals in marine environment is based on the fact that kaolinite, illite, chlorite and smectite generally have different size distributions (Gibbs, 1977). Smectite has the smallest particle size (0.9–0.1 μm) and thus could become enriched after long-distance transport and sorting by oceanic currents. If this is the case in the Yellow Sea, we would expect much higher smectite content in sediments deposited at shallow marine environment since 0.8 Ma than those deposited at terrestrial condition at 3.5–0.8 Ma. However, this is in contrary to our sediment record (Fig. 3). In addition, the dominant diagenetic change of clay minerals is the progressive reaction of smectite to illite, which depends primarily on temperature (Fagel, 2007). In sedimentary deposits characterized by a normal geothermal gradient (~30 °C/km), burial diagenesis of clay minerals operates at depths greater than 2500–3000 m (Chamley, 1989; Fagel, 2007). Both the low geothermal gradient (average 28.6 °C/km) (Yang et al., 2003a) and the shallow burial (<300 m) of sediment on the Yellow Sea continental shelf preclude significant influence of diagenesis on the clay minerals assemblages, which is consistent with the typical detrital morphology (flakes or platy particles with angular borders) of clay minerals at Core CSDP-1 (Fig. 7). Besides, exposure of wide continental shelf during the glaciation might cause subaerial weathering and pedogenesis that could produce “secondary” clay, especially in tropical region (Wan et al., 2017). However, the slight change (<2%) of clay minerals composition at the study core through the last glaciation to the Holocene (Fig. 4) would not help to explain the dramatic decrease (>13%) of smectite from Unit 2 to Unit 1 (Fig. 3 and Table 1). Therefore, we suggest that there is a significant change of the clay-sized sediment source from the paleo-Yangtze River to Yellow River at ~0.8 Ma.

Sr-Nd isotope data are also used to constrain the sediment provenance at Core CSDP-1. The εNd values and, to a lesser extent, the $^{87}Sr/^{86}Sr$ values can be used as reliable tracers for identifying the source of sediments as they mainly depend on lithologies and rock ages (e.g., Goldstein and Jacobsen, 1988; Grousset and Biscaye, 2005; Lupker et al., 2013). The distinctive source rocks and weathering processes that contrast between the modern Yellow and Yangtze River catchments could account for their difference in Sr-Nd isotopic compositions (e.g., Hu et al., 2012; Meng et al., 2008; Yang et al., 2007a). As there is no significant change in Nd isotope compositions in both Chinese loess sequence (Chen and Li, 2013) or Yangtze River core sediments (Yang et al., 2007b) since the late Pliocene, we assume that the Sr-Nd isotopes of modern Yellow River (Hu et al., 2012) and Yangtze River sediment (Yang et al., 2007a and this study) can roughly represent the end-members of potential sources. Most of the samples from Units 1 and 2 at Core CSDP-1 fall into two separate groups and overlap with the Yellow and Yangtze River sediments, respectively (Fig. 7). Combined with the clay mineral results discussed above, we conclude that the sediments delivered to the study site prior to 0.8 Ma were mainly controlled by the paleo-Yangtze River, and later was dominated by

the Yellow River.

5.4. River evolution and sedimentary response

The Yellow and Yangtze Rivers, as two of the largest rivers in the world, are developed on the northeast and eastern margin of the Tibetan Plateau and now flow into the Bohai Sea and East China Sea, respectively (Fig. 1). However, these river systems are sensitive to change because of the tectonic evolution of the region through which it flows (Lin et al., 2001; Zheng et al., 2013). In this case, either the final integration of each river in their present forms or shifts in the location of the river channel and estuary would be expected to have a significant influence on regional sedimentary environment in the marginal seas.

In response to regional extension of eastern China, surface uplift in eastern Tibet and strengthened East Asian summer monsoon, the Yangtze River has been interpreted to have been established before about 23 Ma and possible flowed into the Subei-South Yellow Sea Basin shortly after that time (Zheng et al., 2013) (Fig. 1). Previous studies of whole rock geochemistry, single mineral chronology, clay mineral and heavy mineralogy from the sediment cores in the modern Yangtze delta suggested that the final integration of Yangtze River into the modern river delta occurred around the late Pliocene to middle Pleistocene, likely in response to continuous uplift of the Tibetan Plateau and accelerated subsidence of the eastern China coast (e.g., Chen et al., 2014; Fan et al., 2005; Gu et al., 2014; Jia et al., 2010; Yang et al., 2006a; Yue et al., 2018). However, these studies cannot exclude the possibility that the major channel of paleo-Yangtze River may have flowed across the northern Jiangsu Basin instead of the modern Yangtze delta before the late Pliocene to middle Pleistocene (Zheng et al., 2013). Data from seismological isopach map across the coastal plain in Eastern China reveal that more than one thousand meters of terrestrial sediment were deposited in the Subei-Southern South Yellow Sea Basin in the Tertiary, but very thin strata (<300 m) were distributed in the modern Yangtze delta (Chen and Stanley, 1995; Qin et al., 1989). In contrast, since the early to middle Pleistocene, the Yangtze River delta depocenter and fluvial channel system has shifted southward from the Subei-South Yellow Sea Basin to the modern Yangtze delta caused by tectonic subsidence of eastern China coast and the Min-Zhe Uplift (Chen and Stanley, 1995; Li et al., 2011a; Qin et al., 1989). Several long boreholes drilled in the Jianghan and Dongting Basins of the middle part of the Yangtze River, revealed very stable provenance and sedimentation rate (~95 m/Ma) since the late Pliocene (Bai et al., 2011; Shao et al., 2012; Zhang et al., 2008), excluding any significant changes in trap effect of sediment within the Yangtze drainage basin through the Quaternary. Therefore, we believe that the remarkable change in thickness of strata in Subei-South Yellow Sea Basin and the modern Yangtze delta just reflects the migration of river mouth. The southward migration of the river delta is consistent with the rapid decrease in sediment supply from the Yangtze River to the South Yellow Sea at ~0.8 Ma, as shown by the abrupt change in clay mineral assemblages and Sr-Nd isotopes at our study core (Fig. 3).

The current course of the Yellow River has an unusual 1500-km-long angular bend around the Ordos tectonic block. The sedimentary and tectonic evidence imply that the Yellow River formed in the Eocene and developed its square bend in the late Miocene-early Pliocene (Lin et al., 2001). This square bend and the extensional grabens were the consequence of uplift of the northeastern Tibetan Plateau uplift and compressional tectonic deformation along its margin (Lin et al., 2001; Pan et al., 2011). However, geochronological study of the Gonghe Basin (Fig. 1) in the upper reaches of the Yellow River suggested that headward basin integration occurred at 0.5–1.8 Ma (Craddock et al., 2010). Moreover, many studies from the Sanmenxia Gorge (Fig. 1), the last gorge within the major course before the Yellow River flows into the sea, also imply a similar younger age for the final integration of the Yellow River (0.9–1.4 Ma) (e.g., Hu et al., 2017; Kong et al., 2014; Li et al., 2017; Pan et al., 2005). This age is approximately consistent with the timing of the initial influence of Yellow River-derived sediments to the Yellow Sea as revealed in this study, as well as the results of Yang et al. (2001) and Yao et al. (2017) from the Yellow River delta and central Yellow Sea, respectively. That means that Yellow River sediments have influenced the Yellow Sea at least since the middle Pleistocene. However, we emphasize that this study does not exclude a possible older age for the birth of the Yellow River because the sediment core here only extends to ~3.5 Ma and the paleo-Yellow River could also possibly flow into the Bohai Sea before the late Pliocene (Yao et al., 2017). Such hypothesis can only be tested by future deeper drilling in the Bohai and Yellow Seas.

5.5. Links to tectonic uplift or climate change?

The approximate consistency in timing of the provenance transition from the Yangtze River to Yellow River and onset of large-scale regional transgression in the Yellow Sea at ~0.8 Ma is intriguing, and possibly suggests a causal link between evolution of the river system and sedimentary basins with tectonic evolution and/or climate change. Some studies argue that the final integration of the Yellow River basin was the result of a climatically driven expansion of lake systems since the mid-Pleistocene transition (MPT), rather than major control by tectonic processes (Craddock et al., 2010; Kong et al., 2014; Yao et al., 2017). This is because the onset of rapid incision of the Yellow River roughly coincides with increased amplitude of climate change across MPT. Furthermore, the age of incision significantly lags the growth of high topography in northeastern Tibet at 14–8 Ma. Intuitively stronger monsoon precipitation or enhanced glacial-interglacial contrasts in climate conditions might be expected intensify erosion and river incision (Zhang et al., 2001).

However, this interpretation cannot exclude the possible influence of tectonic deformation. The development of fluvial systems in East Asia is closely linked to the evolving topography and Tibetan uplift, as crustal deformation created regional elevated terrain that provides potential energy to rivers and glaciers, the main agents of erosion (Clark et al., 2004; Zheng et al., 2013). The dating of late Cenozoic basin sediments and the tectonic geomorphology of the NE Tibetan Plateau demonstrates that rapid persistent rise of the plateau began at the Miocene followed by stepwise accelerated rise at ~3.6 Ma, 2.6 Ma, 1.7 Ma, 1.2–0.6 Ma and 0.15 Ma, named the Qing-Zang Movement (QZM A and B), Kunlun-Huanghe Movement (KHM) and Gonghe Movement (GHM) (Fig. 8G) (Jia et al., 2017; Li et al., 2014a; Zhang et al., 2017). These stepwise tectonic uplift and deformation events in NE Tibet are suggested to have been the major driver of the rapid incision of Yellow River at ~1.8–1.4 Ma, 1.2–0.8 Ma and ~0.15 Ma (Jia et al., 2017; Li et al., 2014a; Zhang et al., 2017) (Fig. 8F and G), as well as the final integration of modern Yangtze River (e.g., Chen et al., 2014; Fan et al., 2005; Gu et al., 2014; Jia et al., 2010; Yang et al., 2006a) and subsidence of eastern China coast since the late Pliocene or middle Pleistocene (Chen and Stanley, 1995; Gu, 2015; Yue et al., 2018). The inherent mechanism and consistent timing between tectonic deformation and river evolution strongly suggests their close links, as demonstrated in many previous studies (Clark et al., 2004; Clift et al., 2006; Zheng et al., 2013).

Moreover, it is difficult to use climate change to explain the agreement in timing of the provenance shift from the Yangtze River to Yellow River and onset of large-scale regional transgression in the Yellow Sea at ~0.8 Ma. The nearly synchronous evolution of the

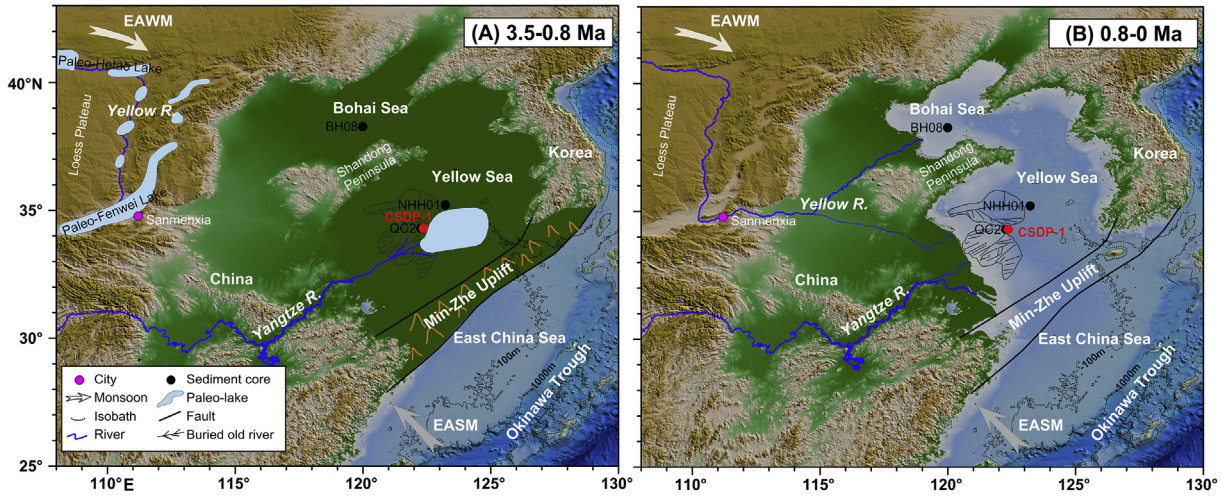

Fig. 9. Time scales of tectonic schematic diagrams illustrate the evolution of the Yellow River, the Yangtze River as well as the Bohai and Yellow Seas. (A) During 3.5–0.8 Ma, the paleo-Yellow River was in a form of a series of isolated paleolakes and poured into the paleo-Hetao lake and paleo-Fenwei lake (Hu et al., 2017; Li et al., 2017; Pan et al., 2011), the paleo-Yangtze River direct flowed into the South Yellow Sea Paleo-lake according to the sedimentary sequence around the South Yellow Sea (Li et al., 2011a; Liu et al., 2014; Liu et al., 2018; and this study), and fluvial/lacustrine deposits were prevail in the Bohai and Yellow Seas due to the barrier of the Min-Zhe Uplift (Liu et al., 2018; Qin et al., 1989; and this study). (B) During 0.8–0 Ma, the Yellow River integrated and input into the Bohai and/or Yellow Seas (Hu et al., 2017; Yang et al., 2001; Yao et al., 2017; and this study), the Yangtze River migrated to the modern Yangtze River Delta (Chen and Stanley, 1995; Li et al., 2011a), and the Bohai and Yellow Seas controlled by global sea-level due to the tectonic subsidence of Min-Zhe Uplift (Liu et al., 2018; and this study). Buried late mid-Pleistocene paleo-rivers systems in the Yellow Sea are modified from Zhang et al. (2013) and showed by gray line.

Yellow/Yangtze River and Min-Zhe Uplift tectonic subsidence at the mid-Pleistocene can only be forced by tectonic processes. Based on above review about river evolution and its possible links, we can propose a schematic regime (Fig. 9) that the uplift of northeastern Tibet at the late Plio-Pleistocene (Li et al., 2014a) together with increased climate variability (Zhang et al., 2001), induced the evolution of large rivers drainage system and the tectonic subsidence of eastern marginal seas (Chen and Stanley, 1995). Uplift of the eastern Tibet and regional extension faulting in the Loess Plateau region coupled with subsidence of basins across eastern China not only opened a path for the Yellow River flowing to the east (Hu et al., 2017; Li et al., 2014a), but also removed the relief barrier of the Pacific water northward intrusion to the Yellow Sea since about 0.8 Ma. These changes in river systems and sedimentary environment in Eastern China Sea before and after the middle Pleistocene are simplified in two schematic diagrams (Fig. 9A and B). Therefore, we conclude that tectonic deformation, rather than climate change, is the first-order factor control the evolution history of the Yellow and Yangtze Rivers and environmental change in the Bohai and Yellow Seas.

6. Conclusions

In order to reveal the evolution of sediment provenance and paleoenvironment of the Yellow Sea, we analyzed clay mineralogy and Sr-Nd isotopic compositions of the <63 μm silicate sediment from Core CSDP-1 from the western South Yellow Sea. We conclude that comparison of the regional marine transgression shows that onset of large-scale transgression in the Yellow and Bohai Seas during the Quaternary is roughly synchronous and occurred consistently since ~0.8 Ma, possibly controlled by tectonic subsidence of eastern China coast and the Min-Zhe Uplift.

Sediments delivered to the study site prior to 0.8 Ma was mainly derived from the paleo-Yangtze River, and was later dominated by the Yellow River. Combined with the previous studies about the evolution of the Yellow and Yangtze Rivers, we suggest that Yellow River sediments began to influence the Yellow Sea no later than the middle Pleistocene.

Climate change by itself cannot explain the general consistence in timing of the provenance shift from the Yangtze River to Yellow River and onset of large-scale regional transgression in the Yellow Sea at ~0.8 Ma. We suggest that the uplift of northeastern Tibet at the late Plio-Pleistocene, together with increased climate variability across MPT, induced the evolution of large rivers drainage system and the tectonic subsidence of eastern marginal seas.

Acknowledgments

We acknowledge the Chinese Continental Shelf Drilling Program and the scientific party and technicians of Core CSDP-1 for recovering the samples. We are grateful to Dr. Youbin Sun for his kind providing the loess samples and Xuejun Jiang for SEM analysis. We thank Pengyuan Guo, Junjie Zhang and Jinhua Shi for the assistance in isotope analyses. We thank the editor Ingrid Hendy and two anonymous reviewers for their constructive comments. This work was supported by the National Natural Science Foundation of China (41622603, 41576034, U1606401), National Program on Global Change and Air-Sea Interaction (GASI-GEOGE-03), Innovation Project (2016ASKJ13, MGQNLM-TD201805), Taishan and Aoshan Talents program (2017ASTCP-ES01) of Qingdao National Laboratory for Marine Science and Technology and Continental Shelf Drilling Program (DD20160147, DD20190208).

Appendix A. Supplementary data

Supplementary data to this article can be found online at https://doi.org/10.1016/j.quascirev.2019.06.002.

References

Bai, D.Y., Chang-An, L.I., Chen, D.P., Zhou, K.J., Huang, W.Y., 2011. Chemical weathering index and magnetic susceptibility of deposits and their responses to the Quaternary climate in Dongting Basin (in Chinese). Chin. Geol. 38, 779–785.
Biscaye, P.E., 1965. Mineralogy and sedimentation of recent deep-sea clay in the Atlantic Ocean and adjacent seas and oceans. Geol. Soc. Am. Bull. 76, 803–832.
Chamley, H., 1989. Clay Sedimentology. Springer, New York.
Chen, J., Wang, Z.H., Wei, T.Y., Zhao, B.C., Chen, Z.Y., 2014. Clay minerals in the Pliocene-Quaternary sediments of the southern Yangtze coast, China: sediment

sources and palaeoclimate implications. J. Palaeogeogr. 3, 297–308.
Chen, Z., Li, G., 2013. Evolving sources of eolian detritus on the Chinese Loess Plateau since early Miocene: tectonic and climatic controls. Acta Cosmologica Earth Planet. Sci. Lett. 371, 220–225.
Chen, Z., Stanley, D.J., 1995. Quaternary subsidence and river channel migration in the Yangtze delta plain, eastern China. J. Coast. Res. 11, 927–945.
Cho, H.G., Kim, S.O., Kwak, K.Y., Choi, H., Khim, B.K., 2015. Clay mineral distribution and provenance in the Heuksan mud belt, Yellow Sea. Geo Mar. Lett. 35, 411–419.
Chung, S.-L., Jahn, B.-m., 1995. Plume-lithosphere interaction in generation of the Emeishan flood basalts at the Permian-Triassic boundary. Geology 23, 889–892.
Clark, M.K., Schoenbohm, L.M., Royden, L.H., Whipple, K.X., Burchfiel, B.C., Zhang, X., Tang, W., Wang, E., Chen, L., 2004. Surface uplift, tectonics, and erosion of eastern Tibet from large-scale drainage patterns. Tectonics 23, 1–20.
Clift, P.D., Blusztajn, J., Nguyen, A.D., 2006. Large-scale drainage capture and surface uplift in eastern Tibet–SW China before 24 Ma inferred from sediments of the Hanoi Basin, Vietnam. Geophys. Res. Lett. 33, 1–4.
Clift, P.D., Hodges, K.V., Heslop, D., Hannigan, R., Van Long, H., Calves, G., 2008. Correlation of Himalayan exhumation rates and Asian monsoon intensity. Nat. Geosci. 1, 875–880.
Craddock, W.H., Kirby, E., Harkins, N.W., Zhang, H., Shi, X., Liu, J., 2010. Rapid fluvial incision along the Yellow River during headward basin integration. Nat. Geosci. 3, 209–213.
Deng, K., Yang, S., Li, C., Su, N., Bi, L., Chang, Y.P., Chang, S.C., 2017. Detrital zircon geochronology of river sands from Taiwan: implications for sedimentary provenance of Taiwan and its source link with the east China mainland. Earth Sci. Rev. 164, 31–47.
Dessert, C., Dupré, B., Gaillardet, J., François, L.M., Allegre, C.J., 2003. Basalt weathering laws and the impact of basalt weathering on the global carbon cycle. Chem. Geol. 202, 257–273.
Esquevin, J., 1969. Influence de la composition chimique des illites sur leur cristallinité. Bull. Centre Rech. Pau-SNPA 3, 147–153.
Fagel, N., 2007. Chapter four clay minerals, deep circulation and climate. Develop. Marine Geol. 1, 139–184.
Fan, D., Li, C.X., Yokoyama, K., Zhou, B., Li, B., Wang, Q., 2005. Monazite age spectra in the Late Cenozoic of the Changjiang delta and its implication on the Changjiang run-through time. Sci. China D Earth Sci. 1, 1718–1727.
Fan, D., Yang, Z., Mao, D., Guo, Z.-g., 2001. Clay minerals and geochemistry of the sediments from the Yangtze and yellow rivers. Mar. Geol. Quat. Geol. 21, 7–12 (in Chinese).
Folk, R., Andrews, P.B., Lewis, D., 1970. Detrital sedimentary rock classification and nomenclature for use in New Zealand. N. Z. J. Geol. Geophys. 13, 937–968.
Gibbs, R.J., 1977. Clay mineral segregation in the marine environment. J. Sediment. Res. 47, 237–243.
Goldstein, S.J., Jacobsen, S.B., 1988. Nd and Sr isotopic systematics of river water suspended material: implications for crustal evolution. Earth Planet. Sci. Lett. 87, 249–265.
Grousset, F.E., Biscaye, P.E., 2005. Tracing dust sources and transport patterns using Sr, Nd and Pb isotopes. Chem. Geol. 222, 149–167.
Gu, J., 2015. Tectonic subsidence analysis of Subei Basin and Yangtze delta from the Pliocene. Geol. Sci. Technol. Inf. 34, 95–106 (in Chinese).
Gu, J., Chen, J., Sun, Q., Wang, Z., Wei, Z., Chen, Z., 2014. China's Yangtze delta: geochemical fingerprints reflecting river connection to the sea. Geomorphology 227, 166–173.
Guo, Y., Li, Y., Xu, D., Liu, X., Zhang, X., 1997. Tectonic evoluction of Yellow Sea, east China sea and continental shelf and adjacent areas. Mar. Geol. Quat. Geol. 17, 1–12 (in Chinese).
Gylesjö, S., Arnold, E., 2006. Clay mineralogy of a red clay–loess sequence from Lingtai, the Chinese Loess Plateau. Glob. Planet. Chang. 51, 181–194.
Han, Z., Li, X., Chen, Y., 2009. Evolution of sedimentary environment of Neogene gravel beds near Nanjing. Quat. Sci. 29, 361–369 (in Chinese).
Hanebuth, T.J., Voris, H.K., Yokoyama, Y., Saito, Y., Okuno, J.i., 2011. Formation and fate of sedimentary depocentres on Southeast Asia's Sunda Shelf over the past sea-level cycle and biogeographic implications. Earth Sci. Rev. 104, 92–110.
Hu, B., Li, G., Li, J., Bi, J., Zhao, J., Bu, R., 2012. Provenance and climate change inferred from Sr-Nd-Pb isotopes of late Quaternary sediments in the Huanghe (Yellow River) Delta, China. Quat. Res. 78, 561–571.
Hu, Z.B., Pan, B.T., Bridgland, D., Vandenberghe, J., Guo, L.Y., Fan, Y.L., Westaway, R., 2017. The linking of the upper-middle and lower reaches of the Yellow River as a result of fluvial entrenchment. Quat. Sci. Rev. 166.
Jacobsen, S.B., Wasserburg, G., 1980. Sm-Nd isotopic evolution of chondrites. Earth Planet. Sci. Lett. 50, 139–155.
Jia, J.T., Zheng, H.B., Huang, X.T., Wu, F.Y., Yang, S.Y., Wang, K., He, M.Y., 2010. Detrital zircon U-Pb ages of late cenozoic sediments from the Yangtze delta:implication for the evolution of the Yangtze River. Chin. Sci. Bull. 55, 1520–1528.
Jia, L., Hu, D., Wu, H., Zhao, X., Chang, P., You, B., Zhang, M., Wang, C., Ye, M., Wu, Z., 2017. Yellow river terrace sequences of the gonghe–guide section in the northeastern qinghai–Tibet: implications for Plateau uplift. Geomorphology 295, 323–336.
Jiang, F., Fu, J., Wang, S., Sun, D., Zhao, Z., 2007. Formation of the Yellow River, inferred from loess–palaeosol sequence in Mangshan and lacustrine sediments in Sanmen Gorge, China. Quat. Int. 175, 62–70.
Jin, X., 1992. Marine Geology of the East China Sea. China Ocean Press, Beijing, pp. 1–22 (in Chinese).
Jonell, T.N., Li, Y., Blusztajn, J., Giosan, L., Clift, P.D., 2018. Signal or noise? Isolating grain size effects on Nd and Sr isotope variability in Indus delta sediment provenance. Chem. Geol. 485, 56–73.
Kong, P., Jia, J., Zheng, Y., 2014. Time constraints for the Yellow river traversing the Sanmen gorge. Geochem. Geophys. Geosyst. 15, 395–407.
Li, B., Sun, D., Xu, W., Wang, F., Liang, B., Ma, Z., Wang, X., Li, Z., Chen, F., 2017. Paleomagnetic chronology and paleoenvironmental records from drill cores from the Hetao Basin and their implications for the formation of the Hobq Desert and the Yellow River. Quat. Sci. Rev. 156, 69–89.
Li, B., Wei, Z., Li, X., He, Z., Zhang, K., Wang, Z., 2011a. Records from quaternary sediment and palaeo-environment in the Yangtze River delta. Quat. Sci. 31, 316–325 (in Chinese).
Li, G., Hartmann, J., Derry, L.A., West, A.J., You, C.F., Long, X., Zhan, T., Li, L., Li, G., Qiu, W., Li, T., Liu, L., Chen, Y., Ji, J., Zhao, L., Chen, J., 2016. Temperature dependence of basalt weathering. Earth Planet. Sci. Lett. 443, 59–69.
Li, J., Fang, X., Song, C., Pan, B., Ma, Y., Yan, M., 2014a. Late Miocene–Quaternary rapid stepwise uplift of the NE Tibetan Plateau and its effects on climatic and environmental changes. Quat. Res. 81, 400–423.
Li, J., Hu, B., Wei, H., Zhao, J., Zou, L., Bai, F., Dou, Y., Wang, L., Fang, X., 2014b. Provenance variations in the Holocene deposits from the southern Yellow Sea: clay mineralogy evidence. Cont. Shelf Res. 90, 41–51.
Li, L., Zheng, H., Zhao, L., Zhou, B., Jia, J., He, M., 2011b. Temporal and spatial changes of clay minerals since the Miocene in lower reaches of Yangtze River and Chinese Loess Plateau and their palaeoclimate implications. J. Palaeogeogr. 13, 355–362 (in Chinese).
Lin, A., Yang, Z., Sun, Z., Yang, T., 2001. How and when did the Yellow River develop its square bend? Geology 29, 951–954.
Lisiecki, L.E., Raymo, M.E., 2005. A Pliocene-Pleistocene stack of 57 globally distributed benthic δ18O records. Paleoceanography 20, 1–17.
Liu, J., Liu, Q., Zhang, X., Liu, J., Wu, Z., Mei, X., Shi, X., Zhao, Q., 2016a. Magnetostratigraphy of a long quaternary sediment core in the south Yellow Sea. Quat. Sci. Rev. 144, 1–15.
Liu, J., Shi, X., Liu, Q., Ge, S., Liu, Y., Yao, Z., Zhao, Q., Jin, C., Jiang, Z., Liu, S., Qiao, S., Li, X., Li, C., Wang, C., 2014. Magnetostratigraphy of a greigite-bearing core from the south Yellow Sea: implications for remagnetization and sedimentation. J. Geophys. Res. 119, 7425–7441.
Liu, J., Wang, H., Wang, F., Qiu, J., Saito, Y., Lu, J., Zhou, L., Xu, G., Du, X., Chen, Q., 2016b. Sedimentary evolution during the last ~1.9Ma near the western margin of the modern Bohai Sea. Palaeogeogr. Palaeocl. 451, 84–96.
Liu, J., Zhang, X., Mei, X., Zhao, Q., Guo, X., Zhao, W., Liu, J., Saito, Y., Wu, Z., Li, J., 2018. The sedimentary succession of the last~ 3.50 Myr in the western south Yellow Sea: paleoenvironmental and tectonic implications. Mar. Geol. 399, 47–65.
Lu, J., Li, A., 2015. Seasonal variations and influencing factors of the grain size characteristics of surface sediments in the South Yellow Sea. Mar. Sci. 39, 48–58 (in Chinese).
Lu, J., Li, A., Huang, P., Li, Y., 2015. Mineral distributions in surface sediments of the western South Yellow Sea: implications for sediment provenance and transportation. Chin. J. Oceanol. Limnol. 33, 510–524.
Lupker, M., France-Lanord, C., Galy, V., Lavé, J., Kudrass, H., 2013. Increasing chemical weathering in the Himalayan system since the last glacial maximum. Earth Planet. Sci. Lett. 365, 243–252.
Mcmanus, J., 1988. Grain size determination and interpretation. Tech. Sediment. 408, 63–85.
Meng, X., Liu, Y., Shi, X., Du, D., 2008. Nd and Sr isotopic compositions of sediments from the Yellow and Yangtze Rivers: implications for partitioning tectonic terranes and crust weathering of the Central and Southeast China. Front. Earth Sci. China 2, 418–426.
Miller, K.G., Kominz, M.A., Browning, J.V., Wright, J.D., Mountain, G.S., Katz, M.E., Sugarman, P.J., Cramer, B.S., Christie-Blick, N., Pekar, S.F., 2005. The Phanerozoic record of global sea-level change. Science 310, 1293–1298.
Milliman, J.D., Farnsworth, K.L., 2011. River Discharge to the Coastal Ocean: a Global Synthesis. Cambridge University Press.
Moore, D.M., Reynolds Jr., R.C., 1989. X-ray Diffraction and the Identification and Analysis of Clay Minerals. Oxford University Press.
Pan, B., Hu, Z., Wang, J., Vandenberghe, J., Hu, X., 2011. A magnetostratigraphic record of landscape development in the eastern Ordos plateau, China: transition from late Miocene and early Pliocene stacked sedimentation to late Pliocene and quaternary uplift and incision by the Yellow river. Geomorphology 125, 225–238.
Pan, B., Wang, J., Gao, H., Chen, Y., Li, J., Liu, X., 2005. Terrace dating as an archive of the run-through of the Sanmen Gorges. Prog. Nat. Sci. 15, 1096–1103.
Qiao, S., Shi, X., Wang, G., Zhou, L., Hu, B., Hu, L., Yang, G., Liu, Y., Yao, Z., Liu, S., 2017. Sediment accumulation and budget in the Bohai Sea, Yellow Sea and east China sea. Mar. Geol. 390, 270–281.
Qin, Y., Zhao, Y., Chen, L., Zhao, S., 1989. Geology of the Yellow Sea. Oceanic Publish House, Beijing, pp. 1–289 (in Chinese).
Rea, D.K., Janecek, T.R., 1981. Mass-Accumulation Rates of the Non-authigenic Inorganic Crystalline (Eolian) Component of Deep-Sea Sediments from the Western Mid-Pacific Mountains, Deep Sea Drilling Project Site 463.
Ren, J., Tamaki, K., Li, S., Zhang, J., 2002. Late Mesozoic and Cenozoic rifting and its dynamic setting in Eastern China and adjacent areas. Tectonophysics 344, 175–205.
Ren, M.-e., Shi, Y.-l., 1986. Sediment discharge of the Yellow river (China) and its effect on the sedimentation of the Bohai and the Yellow Sea. Cont. Shelf Res. 6, 785–810.

Révillon, S., Jouet, G., Bayon, G., Rabineau, M., Dennielou, B., Hémond, C., Berné, S., 2011. The provenance of sediments in the gulf of lions, western Mediterranean sea. Geochem. Geophys. Geosyst. 12, 1–20.
Richardson, N.J., Densmore, A.L., Seward, D., Fowler, A., Wipf, M., Ellis, M.A., Yong, L., Zhang, Y., 2008. Extraordinary denudation in the Sichuan Basin: insights from low-temperature thermochronology adjacent to the eastern margin of the Tibetan Plateau. J. Geophys. Res. 113, 1–23.
Saito, Y., Yang, Z., Hori, K., 2001. The Huanghe (Yellow River) and Changjiang (Yangtze River) deltas: a review on their characteristics, evolution and sediment discharge during the Holocene. Geomorphology 41, 219–231.
Schopka, H.H., Derry, L.A., Arcilla, C.A., 2011. Chemical weathering, river geochemistry and atmospheric carbon fluxes from volcanic and ultramafic regions on Luzon Island, the Philippines. Geochem. Cosmochim. Acta 75, 978–1002.
Shao, L., Li, C.a., Yuan, S., Kang, C., Wang, J., Li, T., 2012. Neodymium isotopic variations of the late Cenozoic sediments in the Jianghan Basin: implications for sediment source and evolution of the Yangtze River. J. Asian Earth Sci. 45, 57–64.
Shen, X., Wan, S., France-Lanord, C., Clift, P.D., Tada, R., Révillon, S., Shi, X., Zhao, D., Liu, Y., Yin, X., 2017. History of Asian eolian input to the Sea of Japan since 15 Ma: links to Tibetan uplift or global cooling? Earth Planet. Sci. Lett. 474, 296–308.
Stanley, D.J., Hait, A.K., 2000. Deltas, radiocarbon dating, and measurements of sediment storage and subsidence. Geology 28, 295–298.
Sun, Y., An, Z., 2005. Late Pliocene-Pleistocene changes in mass accumulation rates of eolian deposits on the central Chinese Loess Plateau. J. Geophys. Res. 110, 1–8.
Wageman, J.M., Hilde, T.W., Emery, K., 1970. Structural framework of east China sea and Yellow Sea. Am. Assoc. Petrol. Geol. Bull. 54, 1611–1643.
Wan, S., Clift, P.D., Zhao, D., Hovius, N., Munhoven, G., France-Lanord, C., Wang, Y., Xiong, Z., Huang, J., Yu, Z., Zhang, J., Ma, W., Zhang, G., Li, A., Li, T., 2017. Enhanced silicate weathering of tropical shelf sediments exposed during glacial lowstands: a sink for atmospheric CO2. Geochem. Cosmochim. Acta 200, 123–144.
Wan, S., Li, A., Clift, P.D., Stuut, J.B.W., 2007. Development of the east Asian monsoon: mineralogical and sedimentologic records in the Northern South China Sea since 20Ma. Palaeogeogr. Palaeoclimatol. Palaeoecol. 254, 561–582.
Wang, H., Saito, Y., Zhang, Y., Bi, N., Sun, X., Yang, Z., 2011. Recent changes of sediment flux to the western Pacific Ocean from major rivers in East and Southeast Asia. Earth Sci. Rev. 108, 80–100.
Wang, P., 2004. Cenozoic Deformation and the History of Sea-Land Interactions in Asia. Continent-Ocean Interactions within East Asian Marginal Seas, pp. 1–22.
Wang, P., Li, Q., Li, C., 2014. Geology of the China Seas. Elsevier.
Wang, Y., Zhang, Z., Zhu, D., Yang, J., Mao, L., Li, S., 2006. River-sea interaction and the north Jiangsu plain formation. Quat. Sci. 26, 301–320 (in Chinese).
Wei, J., Shi, X., Xin, C., Zhang, H., 2001. The distribution characteristic of clay mineral in the South Yellow Sea and its implications. Chin. Sci. Bull. 46, 30–33.
Wentworth, C.K., 1922. A scale of grade and class terms for clastic sediments. J. Geol. 30, 377–392.
Xue, C., 1993. Historical changes in the Yellow river delta, China. Mar. Geol. 113, 321–330.
Yang, S., Cai, J., Li, C.X., Deng, B., 2001. New discussion about the run-through time of the Yellow River. Mar. Geol. Quat. Geol. 21, 17–22 (in Chinese).
Yang, S., Hu, S., Cai, D., Feng, X., Gao, L., Lu, J., 2003a. Geothermal field and thermotectonic evolution in Southern South Yellow Sea basin. Chin. Sci. Bull. 48, 2466–2471.
Yang, S., Jiang, S., Ling, H., Xia, X., Sun, M., Wang, D., 2007a. Sr-Nd isotopic compositions of the Changjiang sediments: implications for tracing sediment sources. Sci. China D Earth Sci. 50, 1556–1565.
Yang, S., Jung, H.S., Li, C., 2004. Two unique weathering regimes in the Changjiang and Huanghe drainage basins: geochemical evidence from river sediments. Sediment. Geol. 164, 19–34.
Yang, S., Li, C., Yokoyama, K., 2006a. Elemental compositions and monazite age patterns of core sediments in the Changjiang Delta: implications for sediment provenance and development history of the Changjiang River. Earth Planet. Sci. Lett. 245, 762–776.
Yang, S.Y., Jung, H.S., Lim, D.I., Li, C.X., 2003b. A review on the provenance discrimination of sediments in the Yellow Sea. Earth Sci. Rev. 63, 93–120.
Yang, S.Y., Wei, G., Xia, X.-P., Sun, M., Tang, M., 2007b. Provenance study of the late Cenozoic sediments in the Changjiang delta: REE and Nd isotopic constraints. Quat. Sci. 27, 339–346 (in Chinese).
Yang, Z., Wang, H., Saito, Y., Milliman, J.D., Xu, K., Qiao, S., Shi, G., 2006b. Dam impacts on the changjiang (Yangtze) river sediment discharge to the sea: the past 55 years and after the three gorges dam. Water Resour. Res. 42, 1–10.
Yao, Z., Shi, X., Qiao, S., Liu, Q., Kandasamy, S., Liu, J., Liu, Y., Liu, J., Fang, X., Gao, J., 2017. Persistent effects of the Yellow River on the Chinese marginal seas began at least~ 880 ka ago. Sci. Rep. 7, 1–11.
Yi, L., Deng, C., Tian, L., Xu, X., Jiang, X., Qiang, X., Qin, H., Ge, J., Chen, G., Su, Q., 2016. Plio-pleistocene evolution of Bohai basin (East Asia): demise of Bohai paleolake and transition to marine environment. Sci. Rep. 6, 29403.
Yi, L., Ye, X., Chen, J., Li, Y., Long, H., Wang, X., Du, J., Zhao, S., Deng, C., 2014. Magnetostratigraphy and luminescence dating on a sedimentary sequence from northern East China Sea: constraints on evolutionary history of eastern marginal seas of China since the Early Pleistocene. Quat. Int. 349, 316–326.
Yi, S., Yi, S., Batten, D.J., Yun, H., Park, S.-J., 2003. Cretaceous and cenozoic non-marine deposits of the northern South Yellow Sea basin, offshore western Korea: palynostratigraphy and palaeoenvironments. Palaeogeogr. Palaeocl. 191, 15–44.
Yoon, Y., Lee, G.H., Han, S., Yoo, D.G., Han, H.C., Choi, K., Lee, K., 2010. Cross-section restoration and one-dimensional basin modeling of the central Subbasin in the southern Kunsan basin, Yellow Sea. Mar. Pet. Geol. 27, 1325–1339.
Yue, W., Jin, B., Zhao, B., 2018. Transparent heavy minerals and magnetite geochemical composition of the Yangtze River sediments: implication for provenance evolution of the Yangtze Delta. Sediment. Geol. 364, 42–52.
Zhang, P., Peter, M., William, R.D., 2001. Increased sedimentation rates and grain sizes 2–4 Myr ago due to the influence of climate change on erosion rates. Nature 410, 891–897.
Zhang, W., Zhang, T., Song, C., Appel, E., Mao, Z., Fang, Y., Lu, Y., Meng, Q., Yang, R., Zhang, D., 2017. Termination of fluvial-alluvial sedimentation in the Xining Basin, NE Tibetan Plateau, and its subsequent geomorphic evolution. Geomorphology 297, 86–99.
Zhang, X., zhang, Z., Lan, X., 2013. The Regional Geological in the South Yellow Sea. China Ocean Press, Beijing (in Chinese).
Zhang, Y., Li, C.a., Wang, Q., Chen, L., Ma, Y., Kang, C., 2008. Magnetism parameters characteristics of drilling deposits in Jianghan Plain and indication for forming of the Yangtze River three gorges. Chin. Sci. Bull. 53, 584–590.
Zhao, D., Wan, S., Jiang, S., Shen, S., Ren, X., Révillon, S., Zhai, L., Dong, J., Zhang, J., Shi, X., 2019. Quaternary sedimentary record in the northern Okinawa Trough indicates the tectonic control on depositional environment change. Palaeogeogr. Palaeocl. 516, 126–138.
Zhao, D., Wan, S., Toucanne, S., Clift, P.D., Tada, R., Révillon, S., Kubota, Y., Zheng, X., Yu, Z., Huang, J., 2017. Distinct control mechanism of fine-grained sediments from Yellow River and Kyushu supply in the northern Okinawa Trough since the last glacial. Geochem. Geophys. Geosyst. 18, 2949–2969.
Zheng, H., Clift, P.D., Wang, P., Tada, R., Jia, J., He, M., Jourdan, F., 2013. Pre-miocene birth of the Yangtze River. P. Natl. Acad. Sci. USA. 110, 7556–7561.
Zhou, M., Ge, Z., 1990. The magnetostratigraphy of unconsolidated sediments in South Yellow Sea and adjacent areas. Mar. Geol. Quat. Geol. 10, 21–32 (in Chinese).